Metabolic Engineering 90 (2025) 92–105

Contents lists available at ScienceDirect

Metabolic Engineering

journal homepage: www.elsevier.com/locate/meteng

The oleaginous yeast *Rhodosporidium toruloides* engineered for biomass hydrolysate-derived (E)-α-bisabolene production

Paul A. Adamczyk [a,b], Hee Jin Hwang [a,b], Ta-Hsuan Chang [e,f], Yuqian Gao [a,c], Edward E.K. Baidoo [a,d,e], Joonhoon Kim [a,c], Bobbie-Jo M. Webb-Robertson [a,c], Javier E. Flores [a,c], Kirch Czarina Quijano [e,f], Meagan C. Burnet [a,c], Nathalie Munoz [a,c], Eric Sundstrom [e,f], John M. Gladden [a,b,d], Di Liu [a,b,*]

[a] *Agile Biofoundry, Emeryville, CA, USA*
[b] *Sandia National Laboratories, Livermore, CA, USA*
[c] *Pacific Northwest National Laboratory, Richland, WA, USA*
[d] *Joint BioEnergy Institute, Emeryville, CA, USA*
[e] *Lawrence Berkeley National Laboratory, Berkeley, CA, USA*
[f] *Advanced Biofuels and Bioproducts Process Development Unit, Emeryville, CA, USA*

ARTICLE INFO

Keywords:
Rhodotorula
Rhodosporidium toruloides
Bisabolene
Mevalonate pathway
Omics
Lignocellulosic hydrolysate

ABSTRACT

The oleaginous yeast *Rhodosporidium toruloides* has been exploited for many bioproducts, including several terpenes, owing to its oleaginous nature and biomass inhibitor tolerance. Here, we built upon previous (E)-α-bisabolene work by iteratively stacking the complete mevalonate pathway from *Saccharomyces cerevisiae* onto a multicopy bisabolene synthase parent strain. Metabolomics and proteomics verified heterologous pathway expression and identified metabolic bottlenecks at three intermediate steps, with candidate feedback-resistant mevalonate kinases screening improving titers 15%. Subtle differences in codon optimization, and preliminary attenuation of competing flux toward lipids resulted in 6-fold, 7-fold higher titers relative to controls, respectively. Media optimization led to modest improvements, with zinc identified as the most promising at 10% titer improvement. Ultimately, high-performance strains were cultivated with corn-stover biomass hydrolysate in microtiter plates at 300 g/L total sugar, achieving 20.8 g/L bisabolene, the highest reported titer in the literature. A 2 L glucose minimal medium bioreactor achieved 19.3 g/L bisabolene and a literature-high productivity of 0.11 g/L/h.

1. Introduction

Biofuels are a potential surrogate to petroleum-based gasoline, diesel, and aviation fuels. Bisabolenes (e.g., (E or Z)-α, *β*-, (E or Z)-γ-bisabolene) are naturally occurring sesquiterpenes widely found amongst plants and fungi—such as the gum resin Opopanax (or bisabol) of the shrub *Commiphora guidottii* (Yeo et al., 2016)—deriving from farnesyl pyrophosphate of the mevalonate and methylerythritol phosphate pathways (Hewage et al., 2023; Spakowicz and Strobel, 2015). Fully saturating bisabolene isomers renders bisabol*ane*, a suitable biodiesel, jet fuel alternative, and fuel additive (Baral et al., 2019; Butcher et al., 2018; Peralta-Yahya et al., 2011) alongside precursor terpenes farnesene, pinene, sabinene, and others (Peralta-Yahya et al., 2012; Walls and Rios-Solis, 2020). While several isomers exist, most metabolic engineering has focused on production of (E)-α-bisabolene (hereafter bisabolene).

Rhodosporidium toruloides (also known as *Rhodotorula toruloides*) is an oleaginous yeast capable of growth on varied carbon sources (Kim et al., 2020; Perez-Pimienta et al., 2019), including acid- and ionic liquid-treated lignocellulosic biomass hydrolysates, and is tolerant to inhibitors thereof (Fernandes et al., 2023; Z. Liu et al., 2021; Yao et al., 2021). *R. toruloides* has high acetyl-CoA flux mainly directed toward triacylglycerol accumulation via lipid droplets, exploited in several studies (Deshavath et al., 2024; Keita et al., 2024; Sunder et al., 2024). Some flux is naturally siphoned toward mevalonate pathway (MVAP)-derived carotenoids such as *β*-carotene, with work focusing on their overproduction (Ochoa-Viñals et al., 2024; Xie et al., 2024). Therefore, *R. toruloides* is well poised for MVAP-derived terpene production

* Corresponding author. Sandia National Laboratories, DOE Agile Biofoundry, 5885 Hollis Street, Fourth Floor, Emeryville, CA, 94608, USA.
E-mail address: diliu@lbl.gov (D. Liu).

https://doi.org/10.1016/j.ymben.2025.02.014
Received 18 October 2024; Received in revised form 18 January 2025; Accepted 28 February 2025
Available online 3 March 2025

evidenced by previous reports of 1,8-cineole, *ent*-kaurene, limonene, prespatane, *epi*-isozizaene, and bisabolene production (Geiselman et al., 2020b, 2020a; Kirby et al., 2021; S. Liu et al., 2021; Zhuang et al., 2019). Of the terpenes showcased in *R. toruloides*, bisabolene has been the most extensively engineered, exploring effects of bisabolene synthase copy number and overexpression of select, metabolomics-derived rate-limiting MVAP transgenes in the context of endogenous MVAP flux and regulation (Kirby et al., 2021; Yaegashi et al., 2017), achieving 2.6 g/L and ~10% of the maximum theoretical yield (MTY) from corn stover biomass hydrolysate (Chen et al., 2016). The titer of this previous best strain was further improved to 7.8 g/L in a 550 mL (250 mL working volume) fed-batch bioreactor of succinic and acetic acid supplemented with yeast extract and peptone (Walls et al., 2023).

Work on bisabolene has been demonstrated in other microbial platforms aside from *R. toruloides*. For example, 180 mg/L in *Synechocystis* sp. PCC 6803 was demonstrated via overexpression of two methylerythritol 4-phosphate pathway (MEPP) enzymes (Rodrigues and Lindberg, 2021). Another example is 12 mg/g CDW in *Methylomicrobium alcaliphilum* 20Z that was achieved through overexpression of three MEPP enzymes with methane as the carbon source (Nguyen et al., 2021). After peroxisomal localization of the MVAP, 1.1 g/L solely from methanol was demonstrated in *Pichia pastoris* (Gao et al., 2024). Furthermore, 5.2 g/L in *Saccharomyces cerevisiae* was achieved implementing three knockouts identified via genome-wide screening for improved carotenoid production in addition to fusing bisabolene synthase to farnesyl diphosphate synthase (ScERG20) to improve its solubility (Özaydın et al., 2013). Moreover, a fed-batch-derived 9.8 g/L bisabolene, 78% MTY (glucose basis), and ~0.08 g/L/h productivity was demonstrated in the purple nonsulfur photosynthetic bacterium *Rhodobacter capsulatus* after overexpressing the heterologous MVAP (from *Paracoccus zeaxanthinifaciens*) alongside endogenous MEPP flux, promoter screening, and knockdown/knockouts of competing pathways to increase FPP and NADPH pools (Zhang et al., 2021). Lastly, *Yarrowia lipolytica* showcased 15.5 g/L bisabolene and ~0.09 g/L/h productivity from waste cooking oil (triacylglycerides) after endogenous MVAP peroxisomal localization and overexpression, introduction of a heterologous efflux pump, enhancing β-oxidation flux, inhibiting fatty acid biosynthesis via cerulenin, and increasing peroxisome count and size (Zhao et al., 2023).

Here, we built upon previous bisabolene work in *R. toruloides* (Kirby et al., 2021) by overexpressing the entire eight-gene MVAP from *S. cerevisiae*—beginning with acetyl-CoA acetyltransferase (ScERG10) and terminating with the promiscuous ScERG20. We tested bisabolene production in small-volume plates and fed-batch bioreactor conditions grown on both corn stover biomass hydrolysate and a glucose synthetic defined medium. We also explored the effects of downregulation of the AcCoA flux toward lipids, media optimization, overexpression of heterologous mevalonate kinases and additional copies of bisabolene synthase, which led to a bisabolene titer of 19.3 g/L and productivity of 0.11 g/L/h in a 2 L bioreactor. This study further establishes *R. toruloides* as a promising host for the production of bisabolene and other biofuels and bioproducts.

2. Materials and methods

2.1. Strains, genotypes, and sequences

Rhodosporidium toruloides (a.k.a. *Rhodotorula toruloides,* a.k.a *Rhodotorula graciis*) IFO 0880 (a.k.a NBRC 0880) was obtained from the Biological Resource Center, NITE (NBRC), Japan. All strains and plasmid sequences in this work are available through the Agile BioFoundry parts registry at https://public-registry.agilebiofoundry.org, and are listed by figure in Additional File 1. Additionally, a visual family tree of all strains is provided in Supplementary Fig. 5. Protein identification numbers used in this manuscript are from the *R. toruloides* genome version 4, available on Mycocosm, the US Department of Energy Joint Genome Institute fungal genome repository (Grigoriev et al., 2014).

For strains constructed by homologous recombination (i.e., targeted integration), the parental strain was a deletion mutant of the non-homologous end-joining factor Ku70 (Koh et al., 2014). Homologous recombination and non-homologous end-joining (i.e., for generating randomly integrated mutants) was achieved by transforming *R. toruloides* with linearized plasmid by a lithium acetate transformation protocol as described in (Otoupal et al., 2019) or TDNA insertion by *Agrobacterium tumefaciens*-mediated transformation as described in (Coradetti et al., 2018), respectively. For strains constructed by random insertion, randomly selected transformants were screened in liquid culture with the appropriate selective agent. Significant variation was observed in growth rates and bisabolene titers amongst transformants, likely a consequence of different levels of expression of the transgenes (and selective markers) due to local chromatin structure, number of integrations, some rate of incomplete partial TDNA integrations, or disruption of important growth processes. Copy numbers of strains mentioned are based upon adding the copy number of the parent strain with the copy number of integrating construct and were not empirically quantified and/or sequenced.

2.2. Media and growth conditions

All chemicals used in this study were from Sigma Aldrich unless otherwise stated. For regular strain maintenance, transformation, and subculturing, cells were grown in 10 g/L yeast extract, 20 g/L peptone, and 20 g/L glucose (YPD). Media recipes used for all figures are listed in Additional File 1. Unless noted otherwise, all overnight strain subculturing was completed in 96 deep-well polypropylene square plates with 500 µL YPD in a Multitron II platform shaker (Infors HT, Annapolis Junction, MD, USA) at 1000 RPM (3 mm orbital radius), 30 °C, 85% relative humidity. All production experiments were started at an initial OD_{600} of 0.1. Optical density was determined by measuring absorbance at 600 nm using a standard cuvette (10 mm lightpath) or a 96-well microtiter plate (normalized to 10 mm lightpath) in a SpectraMax Plus 384 Microplate Reader (Molecular Devices, San Jose, CA, USA). All strains (biological replicates and transformants) were first grown on YPD agar plates (15 g/L agar), with appropriate fungal selection agents followed by picking of individual colonies. Selection marker cassettes with *R. toruloides Tub2* promoter and terminator conferring resistance to hygromycin, G418, nourseothricin, and zeocin at 50, 100, 100, 100 µg/mL, respectively, were used in this study. Concentrated deacetylated, mechanically refined corn stover hydrolysate (DMR) was obtained from the National Renewable Energy Laboratory (Chen et al., 2016). Unless noted otherwise, all experiments were performed in 48-well microtiter plates consisting of 600 µL medium plus 200 µL pentadecane overlay (i.e., 33% overlay; M2P Labs Flower Plate (MTP-48-B)) at 1000 RPM agitation, 30 °C, 85% relative humidity, covered with a breathable AeraSeal film (BS-25), and incubated in a Multitron II platform shaker.

For proteomics and metabolomics preparation in Fig. 8, colonies of *R. toruloides* WT, B13, B16, and B19 were selected in biological quadruplicate from YPD agar and subcultured in YPD overnight. The next day, cells were inoculated into a 48-well flower plate containing a DMR hydrolysate medium with pentadecane overlay at an initial OD_{600} of 0.04 and 0.4 for WT and engineered strains, respectively (to capture strains in the same growth phase at the sample collection time). In addition to each biological replicate, three technical growth replicates were included. Cells were cultured for 46 h, then stopped for intracellular metabolomics extraction and proteomics preparation. For Fig. 7D, biological quadruplicates of B01, B02, and B03 were harvested from a glucose minimal medium at each time point (day 1, 3, and 5) for proteomics.

2.3. Bioreactor cultivations

Pulsed feeding fed-batch fermentation was performed in 2 L

(denoted as R1,3–4)) and 10 L (denoted as R2) double-walled glass bioreactors (BIOSTAT B, Sartorius AG, Goettingen, Germany) equipped with two 6-blade Rushton impellers, a dissolved oxygen (DO) probe (OxyFerm FDA VP 225, Hamilton Bonaduz AG, Bonaduz, Switzerland), and a pH probe (EasyFerm Plus VP 225, Hamilton Bonaduz AG). Dissolved oxygen was maintained at 20% by stir speed (400–1300 RPM for R1,3–4; 317–800 RPM for R2) and air sparging (0.5–2.5 VVM). A 10% solution of Antifoam 204 in water was used to reduce frothing. Temperature was maintained at 30 °C. The pH was maintained at 5 using 10% NH_4OH (R3,1–2) and NaOH (R4). Process values were monitored and recorded using the integrated Sartorius data acquisition software (BioPAT MFCS). Sugar consumption, OD_{600}, and bisabolene production were measured over a period of 262 and 168 h for R3-4 and R1-2, respectively. For R3-4,1–2, there were 800, 800, 700, and 3500 mL of base medium with 270, 270, 270, 1350 mL Durasyn 164, Durasyn 164, dodecane, and dodecane overlay, respectively. The feeding strategies for R3,1–2 were periodic pulsing of a 800 g/L glucose stock solution when glucose was nearly depleted, or 800 g/L glucose and 400 g/L ammonium sulfate (AS) (R4). The feeding was stopped when a certain amount of solution had been added to avoid frothing.

For R3-4, the seed train began with inoculating B22 strain into a culture tube containing 3 mL of YPD. Then, 1% of the cells were transferred to a culture tube with 3 mL of 4-fold diluted base medium in water. This was followed by transferring 1% of the cells to a 1 L baffled flask containing 100 mL of 2-fold diluted base medium in water. The entire 100 mL culture medium was inoculated into one tank for an initial OD_{600} of approximately 0.5. For R1-2, the seed train began with inoculating 0.5 mL B22 from several thawed glycerol stocks (previously grown on YPD plates and saved after growing in YPD medium) into several 250 mL baffled flasks with 50 mL YPD, grown for 1 day, followed by a 100-fold dilution into a second 50 mL YPD 250 mL baffled flask for another day at 30 °C, 200 RPM. These seed cultures were then inoculated at a 10-fold dilution into 200 mL of 2-fold diluted base medium in a 1 L baffled flask at 30 °C, 200 RPM for 1 day. The two bioreactors were then inoculated at an initial OD_{600} of ~0.5 using 100 mL and 500 mL of seed culture for R1 and R2, respectively. Base medium recipes are listed in Additional File 1.

2.4. Metabolomics

After centrifugation and decanting, a fresh equivalent 1 mL of 6 OD_{600} (10 mm path length) worth of biomass underwent quenching and extraction with 300 µL of ice-cold methanol, vortexed for 10 s, followed by 300 µL of ice-cold chloroform with 10 s of vortexing, and finally 150 µL of water was added and vortexed for a final 10 s. Following 4 °C centrifugation at 14000 RCF for 10 min, the top aqueous layer was aspirated and centrifuged through a 500 µL Amicon 3 kDa molecular weight cut-off filter at 4 °C for 30 min (Millipore Sigma, Burlington, MA, USA). After addition of 600 µL water, samples were frozen with liquid nitrogen, lyophilized overnight, resuspended in 100 µL of a 1:1 mixture of LC-MS-grade water and methanol, and transferred to glass vials for analysis. Samples were analyzed alongside MVAP standards using a hydrophilic interaction liquid chromatography time-of-flight mass spectrometry (HILIC-TOF–MS) method described previously (Amer et al., 2022).

2.5. Proteomics

Proteomic samples were prepared based on a previously established protocol (Nakayasu et al., 2016). Global proteomics was performed based on previously established protocol (Liu et al., 2023). Targeted proteomics was performed using liquid chromatography selected reaction monitoring (LC-SRM). Peptides were selected based on their spectra counts in the global proteomics data. All the peptides were further BLASTed to ensure their uniqueness to target proteins in the organism. Crude synthetic heavy isotope-labeled (e.g., 13C/15N on C-terminal lysine and arginine) peptides were purchased from New England Peptide (Gardner, MA) and spiked in the samples at a nominal concentration before LC-SRM analysis. The analysis workflow follows the previously established nanoflow LC-SRM method (Gao et al., 2020).

2.6. Sugar quantification

Sugars were quantified on an Agilent Technologies 1200 series HPLC using an Aminex HPX-87C column (Bio-Rad 1250095) and refractive index detector held at 35 °C. Prior to analysis, samples were diluted to 1:10 and filtered through a 0.45 µM polypropylene membrane microplate filter (Agilent, 200983-100) by centrifugation at 3000 RCF for 3 min. Samples were run for 26 min using an isocratic HPLC-grade water mobile phase at 0.6 mL/min and 85 °C. Quantification was completed via peak area measurements compared to standard curves of pure compounds within their linear range of detection.

2.7. Fatty acid methyl esters (FAME) analysis

Cells equivalent to 1 mL at 10 OD_{600} were harvested and washed with a PBS buffer. Fatty acids were extracted and derivatized to FAMEs using a previously published method (Kim et al., 2020). The samples were centrifuged at 1000 RCF for 1 min to separate the hexane phase, which was collected and diluted 10-fold for analysis by GC-MS (Agilent Intuvo 9000 system with a 5977B mass spectrometer and 7693A autosampler) using a DB-wax UI column (30 m × 0.25 mm × 0.25 µm, Agilent Technologies, USA). The temperature program was: 50 °C for 2 min; ramp to 190 °C at 30 °C/min; increased to 250 °C at 15 °C/min; held at 250 °C for 10 min. The temperatures for the inlet, guard chip, MS transfer line, and MS source were set at 250, 250, 250, and 230 °C, respectively. The carrier gas flow rate was 1.2 mL/min and the injection volume was 1 µL. Data were collected in full scan mode (50–500 m/z), analyzed using MassHunter software, and quantified with a standard curve of ten commercially available high-purity standards (C16:0, C16:1, C17:0, C18:0, C18:1, C18:2, C18:3, C20:0, C22:0, and C24:0).

2.8. Bisabolene quantification

Bisabolene was quantified by adding a known amount of hexadecane into the overlay of all experiments as an internal standard. At the end of culturing, 1 µL of overlay was diluted into 1000 µL of ethyl acetate and analyzed using GC-MS. Bisabolene and hexadecane peaks were integrated with area ratios compared against a standard curve of known mass ratios to peak area ratios of bisabolene to hexadecane. Using the calculated mass ratio and known amount of hexadecane injected at the onset of the experiment, mass and thus titer of bisabolene was determined. GC-MS analysis was performed on a single quadrupole Agilent GC-MS 6890-5973 system (Agilent Technologies, Inc., Santa Clara, CA, USA) equipped with an Agilent DB-5 ms capillary column (30 m length, 0.25 mm diameter, 0.25 µm film thickness) operated in electron impact mode at 70 eV. 1 µL of sample was injected into the GC inlet in split mode (1:20 split ratio) with the GC oven temperature held at 70 °C for 1 min, ramped to 220 °C at 30 °C/min, held for 1 min, with a 1.2 mL/min helium carrier gas flow rate. The injection port and ion source temperatures were maintained at 200 °C and 230 °C, respectively. The mass spectrometer was set to scan mode (m/z range 45–220).

2.9. Quantitative reverse transcription PCR

To verify ACC mRNA down-regulation by the weak promoter candidate, qRT-PCR was carried out in a single tube using Luna® Universal One-Step RT-qPCR Kit (NEB, MA, USA) and CFX96 Touch Real-Time PCR Detection System (BioRad, CA, USA). Mid-log phase cells were used to extract total RNA using RNeasy Kit (Qiagen, Germany) according to the manufacturer's instructions. qRT-PCR conditions were: 45 °C for 10 min, 95 °C for 1 min, followed by 40 cycles of 95 °C for 10 s,

and 60 °C for 30 s, and 65–95 °C for 5 s for the melt curve. ACTIN (RTO4_14107) was used as a reference gene and ACC of B02 was used as a calibrator.

2.10. Maximum theoretical yield calculations

Flux balance analysis was performed using COBRApy (Ebrahim et al., 2013) on the most recent model of *R. toruloides* metabolism (Kim et al., 2020) to calculate the maximum theoretical yields of bisabolene from glucose and xylose by maximizing flux toward bisabolene subject to zero biomass production and lipid accumulation, elimination of manually curated futile NADH/NADPH cycles, and considerations of recent D-xylose metabolism and cofactor usage in *R. toruloides* (Adamczyk et al., 2023). The final calculated values were 0.1983 mol bisabolene per mol xylose and 0.2407 mol bisabolene per mol of glucose.

2.11. Marker recycling

Selected constructs were designed to have a selectable marker in tandem with thymidine kinase from herpes simplex virus, flanked by short homology arms (Alexander et al., 2014). Once successful strains were identified for marker recycling, subculturing in YPD overnight was followed by next-day plating of an aliquot onto the counter-selective plate of YPD agar with 1000 μg/mL 5-fluoro-2-deoxyuridine (FUdR). Thymidine kinase converts the counterselective agent FUdR into fluoro-dUMP, inhibiting thymidylate synthase protein, an essential enzyme converting deoxyuridine monophosphate to deoxythymidine monophosphate in nucleic acid metabolism (Shao et al., 2016). Thus, viable colonies on the selection plates are expected to have spontaneous excision of both the selectable marker and thymidine kinase, which were subsequently verified via PCR and lack of growth on a selective plate containing the targeted marker for recycling.

2.12. Codon optimization

Plasmids with heterologous gene expression were codon optimized via the high-codon adaptation index method (i.e., the most frequently used codons in *R. toruloides'* genome; HC) and using GenScript's in-house codon optimization method (GO). Genes were codon-optimized based on a custom *R. toruloides* IFO0880 codon usage table described in Additional File 1 (Grigoriev et al., 2014).

2.13. Statistical analysis

For all direct comparisons of growth and bisabolene described in the text, we use a 2-tailed independent (equal variance) *t*-test. For statistical analysis of proteomic data we used a combination of parametric (ANOVA with post-hoc Tukey test on intensity scores) and non-parametric tests (G-test on peptide abundance/absence) as previously described for proteomic intensity data with missing values (Webb-Robertson et al., 2010). P-values were then corrected for multiple hypothesis testing with the Benjamini–Hochberg procedure (Benjamini and Hochberg, 1995)

3. Results

3.1. AgBIS and upper MVAP overexpression

To improve bisabolene production, we sought to increase the copy number of the bisabolene synthase and overexpress the mevalonate pathway (Fig. 1). Two vectors, expressing one and three copies of *AgBIS*, respectively, driven by strong native promoters including *Gapdh*, *Ant*, and *Tef1* (Nora et al., 2019) were randomly integrated via AtMT onto the genome of parent strain GB1 from Kirby et al. (2021) already containing 10 copies of *AgBIS* (Fig. 2A). The large variance for both violin plots is typical of AtMT due to contemporaneous exploration of copy number

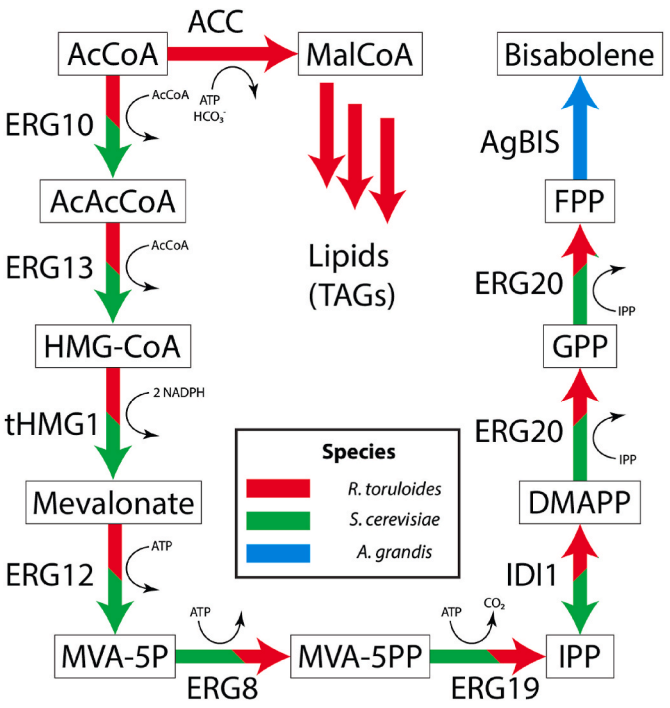

Fig. 1. Map of native *R. toruloides* metabolism overlaid with heterologous MVAP from *S. cerevisiae* and bisabolene synthase integrated in this study. AcCoA, acetyl-CoA; AcAcCoA, acetoAcCoA; HMG-CoA, 3-hydroxy-3-methylglutaryl-CoA; NAD(P)(H), nicotinamide adenine dinucleotide (phosphate) (reduced); MVA-5P, mevalonate-5-phosphate; MVA-5PP, mevalonate-5-pyrophosphate; IPP, isopentenyl pyrophosphate; DMAPP, dimethylallyl pyrophosphate; GPP, geranyl pyrophosphate; FPP, farnesyl pyrophosphate; ATP, adenosine triphosphate; MalCoA, malonyl-CoA; ERG10, acetyl-CoA C-acetyltransferase; ERG13, HMG-CoA synthase; tHMG1, (truncated) HMG-CoA reductase; ERG12, mevalonate kinase; ERG8, phosphomevalonate kinase; ERG19, mevalonate diphosphate decarboxylase; IDI1, IPP delta isomerase 1; ERG20, FPP synthase; AgBIS, bisabolene synthase from *Abies grandis*, ACC, AcCoA carboxylase (RTO4_8639). TAGs (triacylglycerols) are the main component of lipids produced in *R. toruloides*.

and integration sites. The top strain from Fig. 2A (i.e., B09), which contains at least 13 copies of *AgBIS*, was randomly integrated with a construct containing the first three *S. cerevisiae* MVAP genes—*ScERG10*, *ScERG13*, and *SctHMG1*—each driven by strong promoters. We used *S. cerevisiae* MVAP genes since they are proven to yield high-titer strains (Meadows et al., 2016) and can possibly bypass native *R. toruloides* regulation. A truncated version of *ScHMG1* (i.e., *SctHMG1*) was used in this study, which only expresses the soluble catalytic domain of HMG-CoA, and truncates the regulatory transmembrane domain (Donald et al., 1997; Ro et al., 2006). Codon optimization was done via the most frequently used codons in the *R. toruloides* genome (high codon-adaptation index; HC) and GenScript's algorithm (GO). To highlight the robustness and applicability of the engineered strains in the context of a relevant renewable feedstock, transformants were cultured in concentrated DMR (a lignocellulosic hydrolysate prepared from corn stover by deacetylation and mechanical refining followed by enzymatic hydrolysis) at 120 g/L total sugar (2:1 glucose:xylose) (Chen et al., 2016), which yielded very similar final bisabolene titers (Fig. 2B). The top transformant of Fig. 2B (i.e., B11) was isolated and compared against two controls (Fig. 2C). Three DMR recipes explored different buffers and concentrations since *R. toruloides* exhibits pH drops solely with ammonium sulfate (AS) as the nitrogen source, affecting total carbon utilized (Yaegashi et al., 2017). Conversely, pH increases with amino acid and urea-based recipes. 200 mM total phosphate performed the best, although not statistically different amongst top strains. This indicated benefits of controlled pH and/or phosphate nutrient supply. In

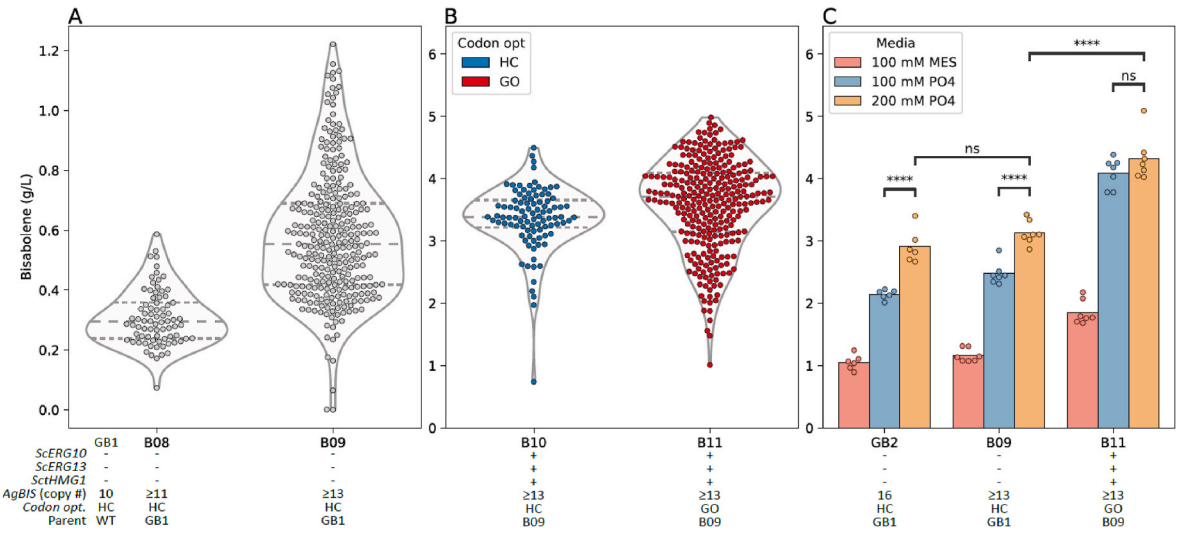

Fig. 2. Effect of additional *AgBIS* copies, codon optimization, partial MVAP integration, and buffers on bisabolene titers. (A) Bisabolene titers of strains over-expressing one or three copies of *AgBIS* in GB1. Left and right violin plots represent n = 78 and n = 286 transformants, respectively, grown on YPD. (B) Bisabolene titers of B10 and B11 strains that expressed the first three *S. cerevisiae* MVAP genes, which were codon optimized via two methods. Left and right violin plots represent 96 and 286 transformants, respectively, grown on DMR. (C) Bisabolene titers of strain B11 compared against two parent strains in DMR media with 3 different buffers. GB1 and GB2 are published strains from Kirby et al. (Kirby et al., 2021). Each plus symbol (+) indicates an independent round of integration of a construct containing the indicated genes. A minus symbol (−) indicates absence of the genotype. Individual points and bar plots represent n = 6 biological replicates and their average, respectively. MES, 2-(N-morpholino)ethanesulfonic acid; PO4, dibasic and monobasic phosphate buffer. ns, $p > 0.05$; *, $0.01 < p \leq 0.05$; **, $0.001 < p \leq 0.01$; ***, $0.0001 < p \leq 0.001$; ****, $p \leq 0.0001$.

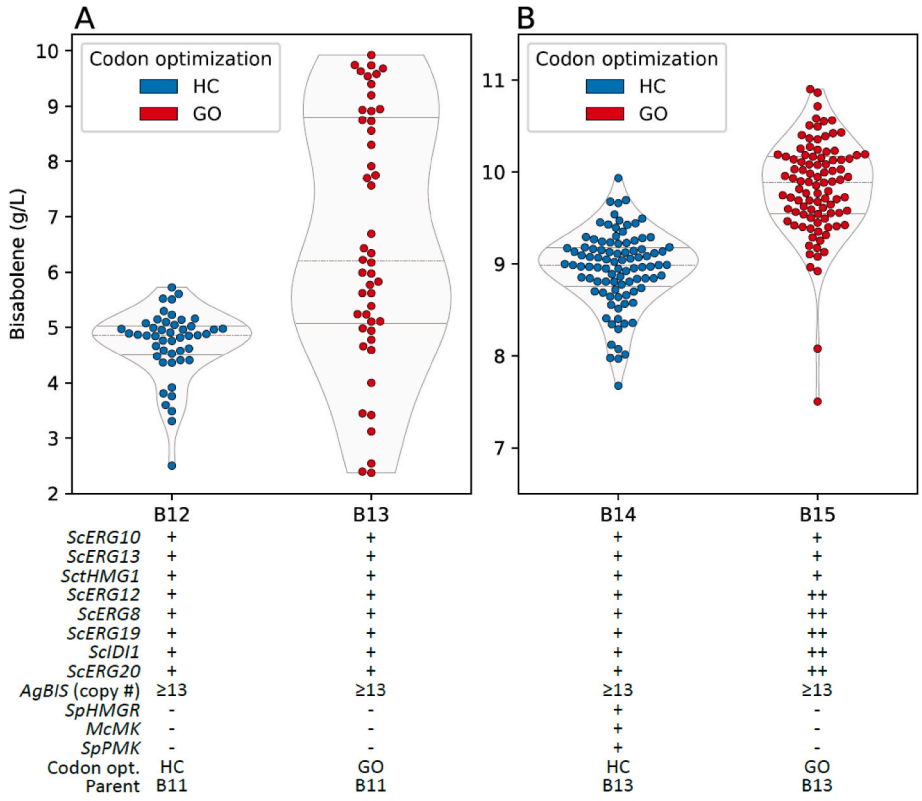

Fig. 3. Effect of codon optimization and combinatorial MVAP integration. (A) Terminal DMR bisabolene titers of individual transformants resulting from random integration of the remaining five *S. cerevisiae* MVAP genes—*ScERG12*, *ScERG8*, *ScERG19*, *ScIDI1*, *ScERG20* in strain B11. Codons are optimized via two methods, HC and GO. Violin plots include n = 47 (left) and 48 (right) individual transformants. (B) Terminal DMR bisabolene titers of individual transformants resulting from random integration of *SpHMGR*, *McMK*, *SpPMK* and the last 5 *S. cerevisiae* MVAP genes in strain B13. Violin plots include n = 96 (left) and 95 (right) individual transformants.

addition to B11, we further selected additional top transformants of Fig. 2B and observed similar behavior (Supp Fig. 1). Strains B11 showed ~50% titer improvement relative to the parent strain (B09) indicating that endogenous MVAP flux was limiting.

3.2. Impact of full MVAP incorporation

The high-performance strain from Fig. 2C (i.e., B11) was randomly integrated with the remaining five genes of the *S. cerevisiae* MVAP—*ScERG12, ScERG8, ScERG19, ScIDI1, ScERG20*, each driven by strong promoters (*Gapdh* and *Tef1*)—via AtMT using the same two codon optimization methods and cultured on ~120 g/L total sugar DMR (Fig. 3A). Unlike Fig. 2B, there was a vast difference between transformants for each codon optimization method utilized, with peak GO titers ~75% higher than peak HC titers. This demonstrated that at least one or more genes greatly benefited from the alternate GO optimization algorithm which, surprisingly, only deviated <3% (DNA sequence) from the HC method. This may be due to mRNA secondary structural differences, mRNA decay rates, and/or a complex multitude of reasons discussed elsewhere (Y. Liu et al., 2021; Trotta, 2013; Tuller and Zur, 2015; Tuller et al., 2010).

With much improvement upon full MVAP integration, additional copies of the last five MVAP genes were randomly integrated into B13 (Fig. 3B). Although partially obfuscated by the increased sugar concentration (150 g/L), titer was not improved, and pointed to imbalanced expression of one or more of the five terminal *S. cerevisiae* genes or a bottleneck upstream.

Previous work from Kirby et al. identified potential metabolic bottlenecks from multi-omics data collected from engineered bisabolene strains (Kirby et al., 2021). Briefly, endogenous HMG1, ERG12, and ERG8 were suspected rate-limiting steps due to poor expression and feedback regulation, and various orthologs were tested—*Methanosaeta concilii* mevalonate kinase (McMK), *Streptococcus pneumoniae* phosphomevalonate kinase (SpPMK), and *Silicibacter pomeroyi* NADH-dependent HMGR (SpHMGR), driven by medium-strong (*Skp1*), medium (*Duf543*), and strong (*Ant*) promoters, respectively—which we randomly integrated into B13 and screened on 150 g/L DMR (Fig. 3B, Additional File 1). Surprisingly, no titer improvement was noted possibly due to low expression.

Fig. 4 shows time-course batch titers of high-performance strains from Fig. 3. Assuming a linear increase in titer from 120 to 150 g/L total sugar, we can infer that B15 does not improve bisabolene yield, similar to Fig. 3. Moreover, maximum productivity for each strain was only 0.066 and 0.054 g/L/h for B13 and B15, respectively, possibly due to the inhibitory and osmotic effects of high DMR sugar concentration and growth defects. Interestingly, productivity of B13 is almost exactly linear, with productivity being equal between days 5, 6 and days 6, 7 (0.066 and 0.065 g/L/h, respectively).

In an attempt to further alleviate pathway bottlenecks and improve bisabolene production, additional combinations of the first three, last five *S. cerevisiae*, and three non-fungal MVAP genes were explored (Fig. 5). The most significant finding is the obvious titer improvement for strains that have the first three MVAP genes integrated twice, highlighting the need for pathway expression balancing.

3.3. Additional bisabolene synthase expression

With optimized combinatorial MVAP overexpression from Fig. 5, we expected an increase in carbon flux through the pathway which may lead to enhanced FPP levels. Thus, overexpression of additional *AgBIS* copies was revisited in the high-performance strain B15 (Fig. 6A), with the best strains compared to the control (Fig. 6B). A total of 96 unique transformants were screened, out of which 5 top strains were selected for further validation. Only B22 showed a modest, statistically significant improvement over the parent B16, indicating that *AgBIS* expression does not seem to be rate limiting at this point.

3.4. Preliminary evaluation of ACC attenuation

Next, as a proof of principle, we sought to mitigate flux toward lipids, the major carbon sink in this organism, which directly competes with bisabolene production for AcCoA (Fig. 1). Essential for growth, AcCoA carboxylase (ACC) can only be attenuated and is the first step in *R. toruloides* TAG accumulation (Castañeda et al., 2018). Therefore, the native *ACC* promoter was replaced by a weak promoter candidate (Pw21; RTO4_15782) mined from transcriptomics data, generating strain B03 (Coradetti et al., 2018; Kim et al., 2020; Nora et al., 2019), that was evaluated for its impact on total fatty acid content and *ACC* transcript levels (Fig. 7A and B). Statistically significant reduced fatty acid content and lowered transcripts were observed in strain B03. Then B03 and B02 (an auxotrophic parent strain of B03 useful for repeated genetic transformations) were integrated with a single copy of *AgBIS* (B05 and B04, respectively) at the *CAR2* locus (RTO4_8589) under the medium-strong constitutive *Gapdh* promoter (Nora et al., 2019) and

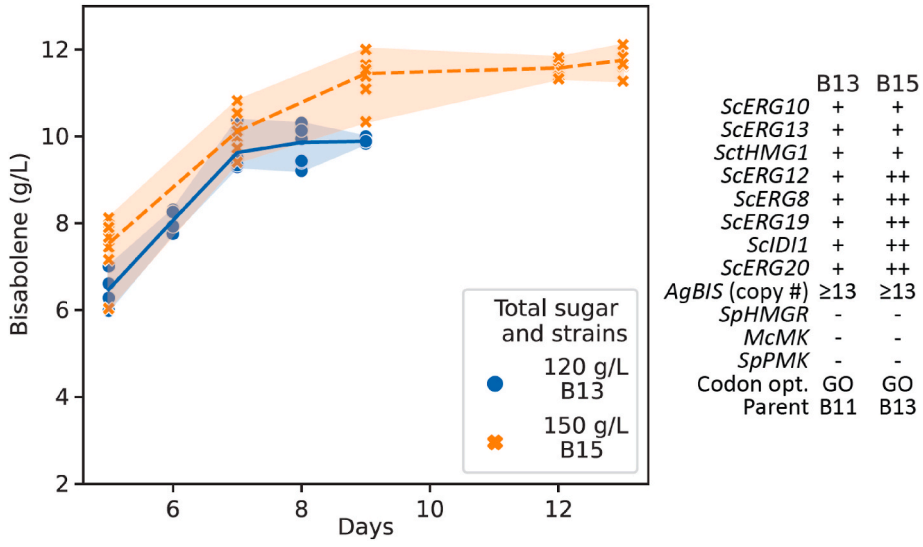

Fig. 4. Titer time course and effect of DMR hydrolysate concentration on bisabolene titers. Solid lines indicate average of biological replicates; solid dots indicate individual data points for each biological replicate (n = 4 and 8 for B13 and B15, respectively) per time point; shaded region indicates 100% percentile interval.

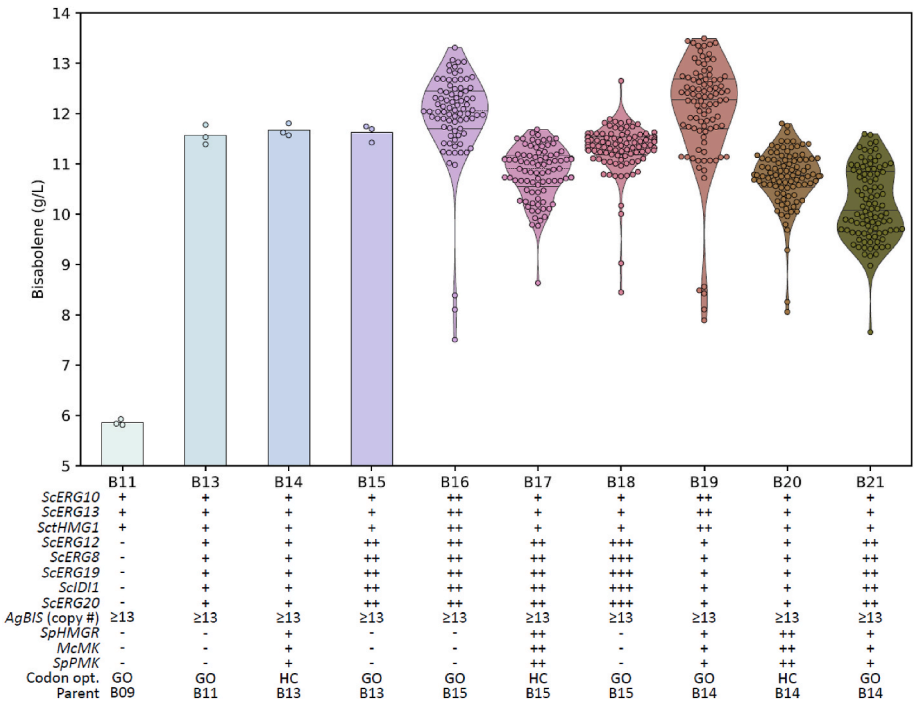

Fig. 5. Effects of combinatorial *S. cerevisiae* MVAP integration on bisabolene titers in DMR hydrolysate. Titers of combinatorial stacking of *S. cerevisiae* MVAP genes in strain B14 and B15 were compared against their parent strains. Bar plots indicate average of biological replicates (n = 3) for a single strain; violin plots include individual transformants (n = 94, 96, 96, 82, 88, and 96).

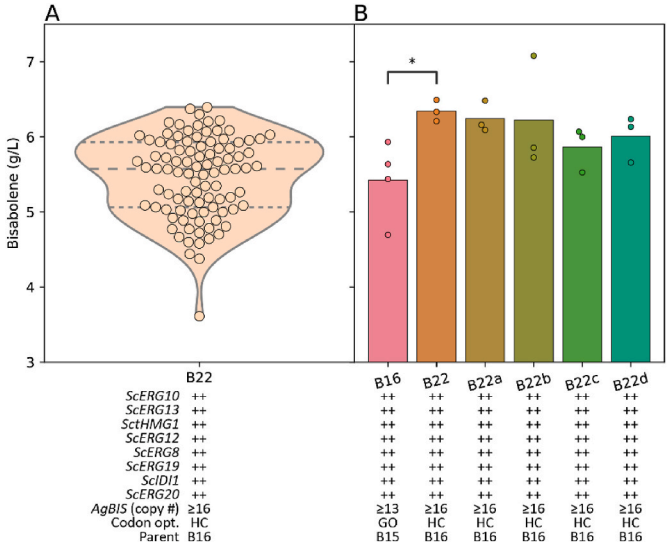

Fig. 6. Effect of additional *AgBIS* copies. (A) Bisabolene titers of parent strain B16 integrated with additional copies of *AgBIS*; individual points represent unique transformants (n = 96). (B) Bisabolene titers of top strains from (A) compared to parent strain B16. All individual points and bar plots represent biological replicates (n = 4) and their average, respectively. ns, $p > 0.05$; *, $0.01 < p \leq 0.05$; **, $0.001 < p \leq 0.01$; ***, $0.0001 < p \leq 0.001$; ****, $p \leq 0.0001$.

tested for bisabolene production, which resulted in a ~7-fold higher titer vs control (Fig. 7C). Finally, targeted proteomics confirmed that B03 ACC levels are lower, with the largest difference of 5.4-fold and 4.1-fold versus B01 (the parent of B02) and B02, respectively, at day 1, and ~2.5-fold lower for days 3 and 5. Likely a compensatory response to the decreased ACC levels, fatty acid synthase complex enzymes (FAS1, FAS2) immediately downstream of ACC, showed ~1.8-fold higher expression in B03.

3.5. Multi-omics analysis

To identify potential bottlenecks, we performed quantitative intracellular metabolomics and proteomics of MVAP metabolites and enzymes on strains from Fig. 5 (Fig 8). Notably, despite high demand (9 mol AcCoA per mol bisabolene) in the engineered strains, intracellular AcCoA levels were relatively stable relative to WT, indicating decent flux toward this node (Fig. 8A). This trend was similar for FPP and combined DMAPP/IPP pools (Fig. 8A). In contrast, MVA was the most accumulated intracellular metabolite, peaking at 90-fold vs WT for B19, but only 2-fold for B13 although sharing a similar titer. This is likely a consequence of the well-documented negative feedback regulation of mevalonate kinases by many organisms from downstream MVAP metabolites, including *S. cerevisiae* (Gray and Kekwick, 1972). Furthermore, the stark increase of MVA in B16 and B19 relative to B13 positively correlates with the number of independent integrations of the first 3 *ScERG* genes. The downstream metabolites (MVA5P, MVA5PP) are relatively more accumulated vs WT (for all strains), prioritizing them as primary bottlenecks. Generally, an imbalanced pathway can lead to diminished thermodynamic driving force and lead to cytotoxicity, as seen in *Escherichia coli* (Martin et al., 2003) and *Bacillus subtilis* (Kazieva et al., 2017; Primak et al., 2011; Sivy et al., 2011). Intracellular HMG-CoA levels are about 15-fold lower and in some replicates, none detected vs WT, suggesting sufficient NADPH reducing power. But without detection of AcAcCoA, it is difficult to conclude if low HMG-CoA levels in the engineered strains are due to unbalanced expression of *ScERG10* and/or *ScERG13* (relative to *tHMGR*). Based on available relative intracellular metabolomics, ScERG19 is the primary bottleneck of the bisabolene production pathway (followed by ScERG8, ScERG12); however, DMAPP/IPP were not separately distinguished and may reveal another bottleneck.

In addition to MVAP intermediates, the energy and redox state of the engineered strains were measured (Fig. 8B). While NADH is not the cofactor used in the MVAP, there was a uniform ~35% increase in cumulative NAD/NADH pools and very different redox ratios relative to WT, a thermodynamic parameter used to calculate *in vivo* flux ratios

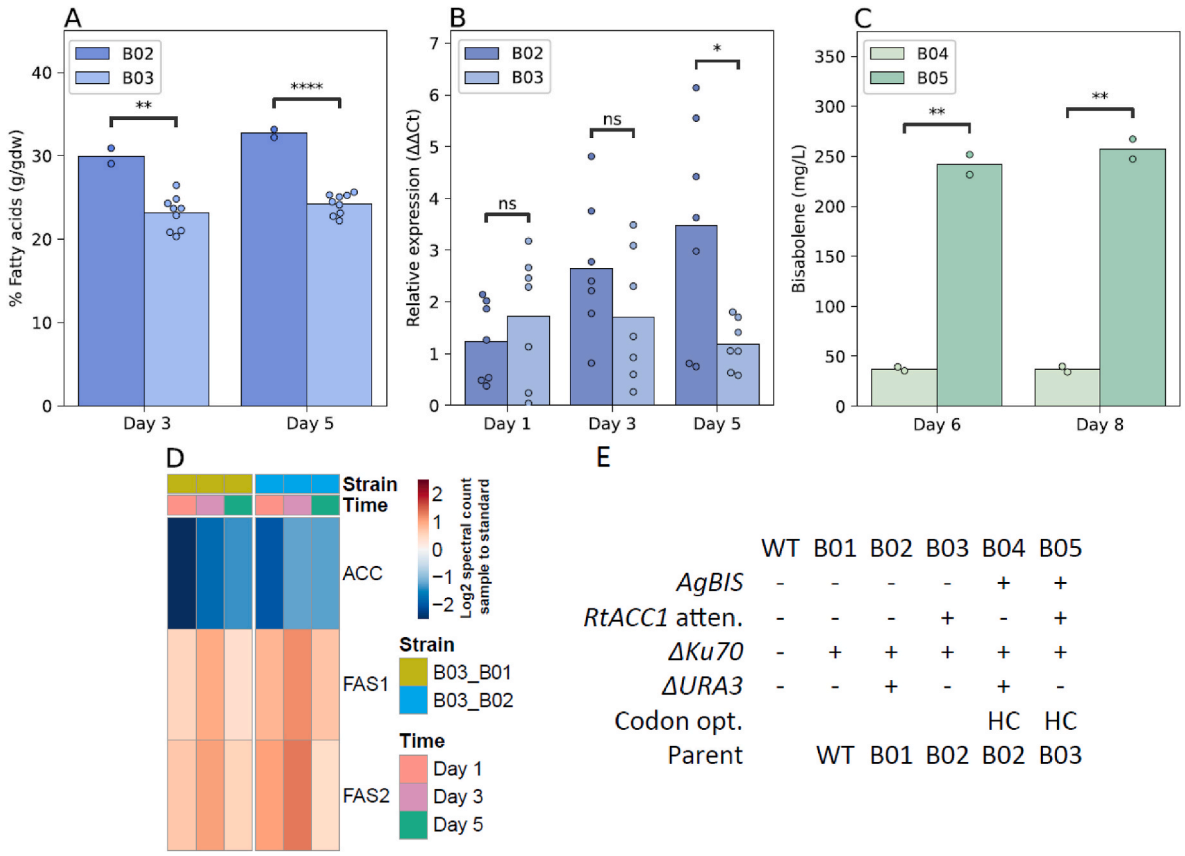

Fig. 7. Assessment of *ACC* weak promoter replacement on mRNA and protein expression, fatty acid and bisabolene production. (A) Averaged total fatty acid profile of B02 (parent) and ACC-attenuated (B03) strains on day 3 and day 5; n = 2 and 9 biological replicates for B02 and B03, respectively. (B) Time-course qRT-PCR to quantify relative *ACC* expression of B02 and B03; n = 9 biological replicates. (C) Bisabolene titers of parent (B04) and *ACC*-attenuated strains (B05) integrated with one copy of *AgBIS* in a DMR medium; n = 2 biological replicates. All individual points and bar plots represent biological replicates and their average, respectively. (D) Targeted proteomics of strains B03 relative to B01 and B02. (E) Genotypes of strains in this figure. ACC, acetyl-CoA carboxylase (RTO4_8639), FAS1, fatty acid synthase β subunit (RTO4_8670); FAS2, fatty acid synthase α subunit (RTO4_8777); n = 4 biological replicates. ns, $p > 0.05$; *, $0.01 < p \leq 0.05$; **, $0.001 < p \leq 0.01$; ***, $0.0001 < p \leq 0.001$; ****, $p \leq 0.0001$.

(forward flux to reverse flux), indicative of reaction efficiency (Park et al., 2016). Specifically, there was a significant increase in the redox ratio of NAD/NADH in B16, B19 strains (44% and 54%, respectively), thermodynamically favoring an increased flux ratio of more oxidative reactions such as glyceraldehyde-3-phosphate dehydrogenase and pyruvate dehydrogenase of lower glycolysis. Interestingly, B13 exhibited an NAD/NADH ratio ~33% lower than WT. These changes in concentration and altered ratios may improve net forward flux through glycolysis to support growth, lipid accumulation, and bisabolene demand. Furthermore, the altered NAD/NADH ratios may also affect *in vivo* redox potential of oxidative phosphorylation and ATP production.

The engineered MVAP and most of TAG biosynthesis pathway utilize NADPH as the required cofactor (6 mol NADPH for 1 mol bisabolene), requiring large flux through oxidative pentose phosphate pathway (OPPP); however, NADPH levels of B16, B19 are very similar to WT (except B13 was ~43% increased).

As for ATP concentrations, all the engineered strains displayed ATP levels ~50% that of WT, a consequence of the high 12 mol ATP for 1 mol of bisabolene demand. Together, these results might inform future engineering strategies such as internal or external redox potential engineering (Lin et al., 2010; Liu et al., 2017).

Targeted and global proteomics (Fig. 8C) demonstrated that all heterologous *S. cerevisiae* MVAP genes were successfully expressed in *R. toruloides*. Notably, the lack of (or very poor) expression of *McMK*, *SpPMK*, and *SpHMGR*, is consistent with the lack of debottlenecking and titer improvement of such strains in Figs. 8A and 5, respectively. Despite multiple rounds of transgene integrations, only *SctHMG1* and *ScERG10* display increased expression relative to B13 (4-fold increase in B16, B19 and 2-fold in B19, respectively). Conversely, the mean expressions of *ScERG8* and *ScERG19* are ~45% and ~35% lower, respectively, in both B16, B19 relative to B13, possibly due to spurious recombination events from repetitive integration of large identical constructs. However, we qualitatively see that the lowest expressed genes (*ScERG12*, *ScERG8*, *ScERG19*) agree well with observed metabolite bottlenecks. Altogether, the marginal titer improvements, excess intracellular MVAP metabolite accumulations, and minimally increased expression levels upon repetitive integrations of the entire *S. cerevisiae* MVAP indicate insufficient expression (and/or activity) of key enzymes, post-translational negative regulation of MVAP enzyme activities from downstream intermediates, and/or other metabolite-driven regulatory mechanisms (Andreassi et al., 2004; Burg and Espenshade, 2011; Dorsey and Porter, 1968; Gray and Kekwick, 1972; Guerra et al., 2021; van der Horst et al., 2020; Voynova et al., 2004). Additionally, aside from the obvious MVAP bottlenecks, we also observed significantly differentially expressed genes in global proteomic data. These include genes related to amino acid metabolism, lipid degradation, and possibly post-translational regulation via acetylation (Supp Fig. 2, Additional File 2). These genes may be promising non-intutive targets for further strain optimization, and further investigation are needed to understand their metabolic implications and identify any potential bottlenecks.

3.6. Heterologous mevalonate kinase expression

With the lack of titer improvement from integration of *SpHMGR*,

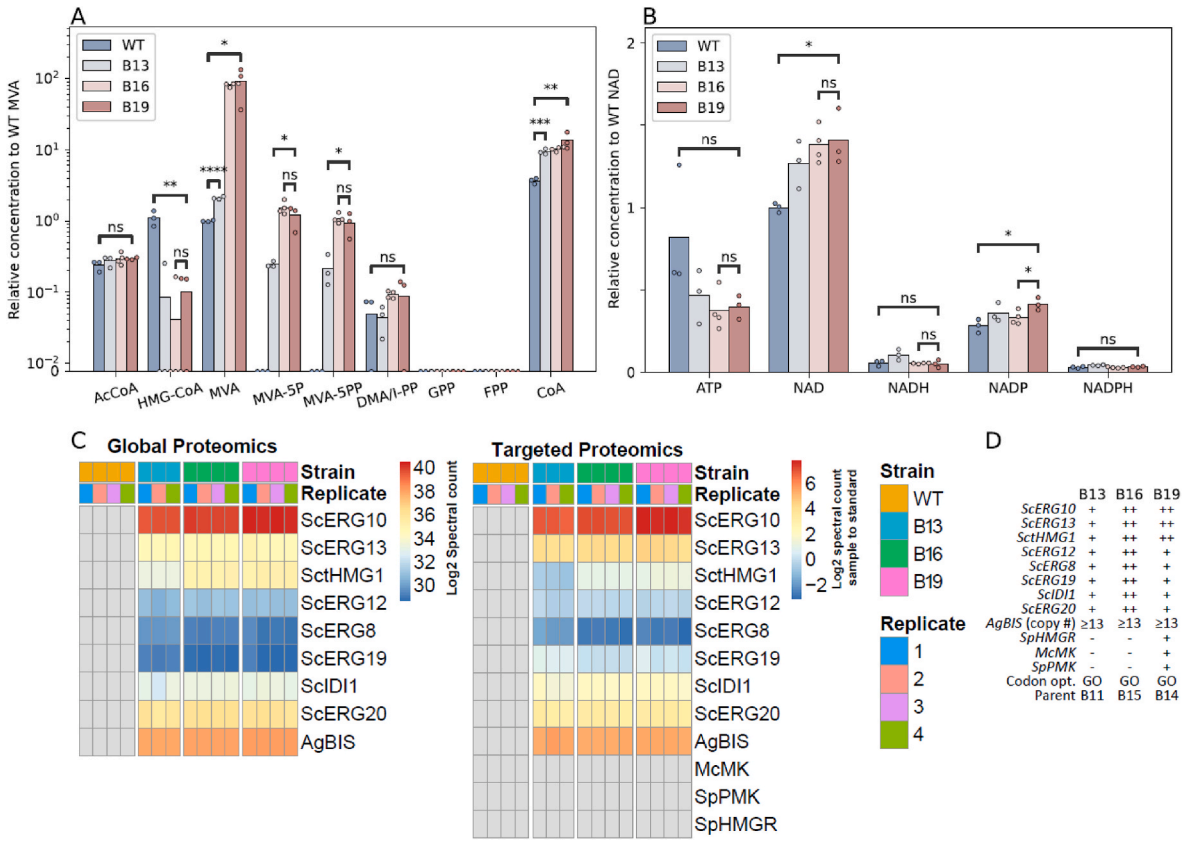

Fig. 8. MVAP metabolomics and proteomics of high-performance strains relative to WT. (A,B) Relative intracellular concentrations of MVAP intermediates, ATP, and cofactors on DMR across different engineered strains vs WT. AcAcCoA could not be detected in this method due to the labile nature of the compound. All individual points and bar plots represent n = 3 biological replicates and their average, respectively. Fig. 8A is a log plot >0.01 and linear from 0 to 0.01 to capture replicates with zero concentration. DMA/I-PP, combined pool of DMAPP and IPP. All concentrations in (A,B) are normalized to the average of WT MVA and NAD, respectively. (C) Global and targeted proteomics of the heterologous *S. cerevisiae* MVAP. Heat maps indicate log2 intensity and log2 ratio of sample to standard intensity, respectively. n = 4 biological replicates. Gray cells, not detected; Sc, *S. cerevisiae*. (D) Genotype of strains depicted. ns, $p > 0.05$; *, $0.01 < p \leq 0.05$; **, $0.001 < p \leq 0.01$; ***, $0.0001 < p \leq 0.001$; ****, $p \leq 0.0001$.

McMK, and *SpPMK* (Fig. 5), additional mevalonate kinases (codon optimized via two methods) were explored in addition to a recently characterized pentose metabolism transcription factor activator (Pnt1) shown to improve fatty alcohol titers and xylose uptake rates (Coradetti et al., 2023) (Fig. 9). All of these transgenes were driven by the same strong *Tef1* promoter from *R. graminis* that has sufficient sequence divergence from the native *Tef1* locus to reduce disruptive integration of the overexpression construct at that locus. Unlike Fig. 3A, codon optimization did not confer any benefit genes screened. Moreover, overexpression of *Pnt1* generally did not improve titers as the improved xylose uptake rates were likely diminished during diauxic growth, demonstrated in Coradetti et al. (2023). Mevalonate kinase from *M. concilii* (Kazieva et al., 2017) tested previously (Fig. 5) with a weaker promoter and codon optimized (via HC) was tested again with a stronger promoter and GO codon optimization, but still did not improve titers (Fig. 9). Mevalonate kinases from *M. mazei* and *M. paludicola* were also tested (Kazieva et al., 2017; Primak et al., 2011), which are feedback resistant to downstream MVAP intermediates, with the top MmMK transformant achieving 14.7 g/L bisabolene, 15% above B16 average titers, and having a peak yield of 36% MTY, the highest in the literature from a biomass hydrolysate.

3.7. Media optimization

Next, we explored the impacts of DMR total sugar concentrations, C:N ratios, trace metals, and alternative nitrogen sources (Supp Fig. 3). Each sugar concentration at 10 g/L ammonium sulfate (AS) yielded the highest average titers (statistically similar to 5 g/L AS), with 150 g/L the highest overall (Supp Fig. 3A). This trend correlates the highest C:N ratios with highest titers (for each sugar concentration), highlighting lipid accumulation during nitrogen starvation likely modulates AcCoA pools, thus MVAP flux (Coradetti et al., 2018; Lopes et al., 2020; Nicaud et al., 2017).

Next, a low-sugar DMR baseline with AS was replaced by alternative nitrogen sources or supplemented with trace metals and vitamins (Supp Fig. 3B). The addition of zinc sulfate was the only statistically significant trace metal that improved titer over baseline. Zinc—an essential cofactor of *E. coli* IDI (Carrigan and Poulter, 2003)—may also directly affect *R. toruloides* MVAP IDI flux. Moreover, zinc is a cofactor involved in lipid synthesis and desaturation, which has dramatically affected *R. toruloides* fatty alcohol titers and is a cofactor of yeast alcohol dehydrogenase (Vallee and Hoch, 1955; Wu et al., 2023). Although not statistically significant, the next three ranked trace components (cadmium chloride, cobalt chloride, silver nitrate) might confer some titer benefit, likely as inhibitors or effects from the conjugate salts. Corn steep solids almost recapitulated baseline titers and warrants further investigation. Lastly, to identify peak batch titers, top strains from Fig. 5 were cultured on 300 g/L total sugar DMR with 10 g/L AS or 10 g/L yeast extract (Fig. 10). Preliminarily, yeast extract is not a suitable AS replacement, at least at 10 g/L. The peak bisabolene titer of 20.8 g/L (25.4% MTY) is the highest titer ever reported in the literature for any organism.

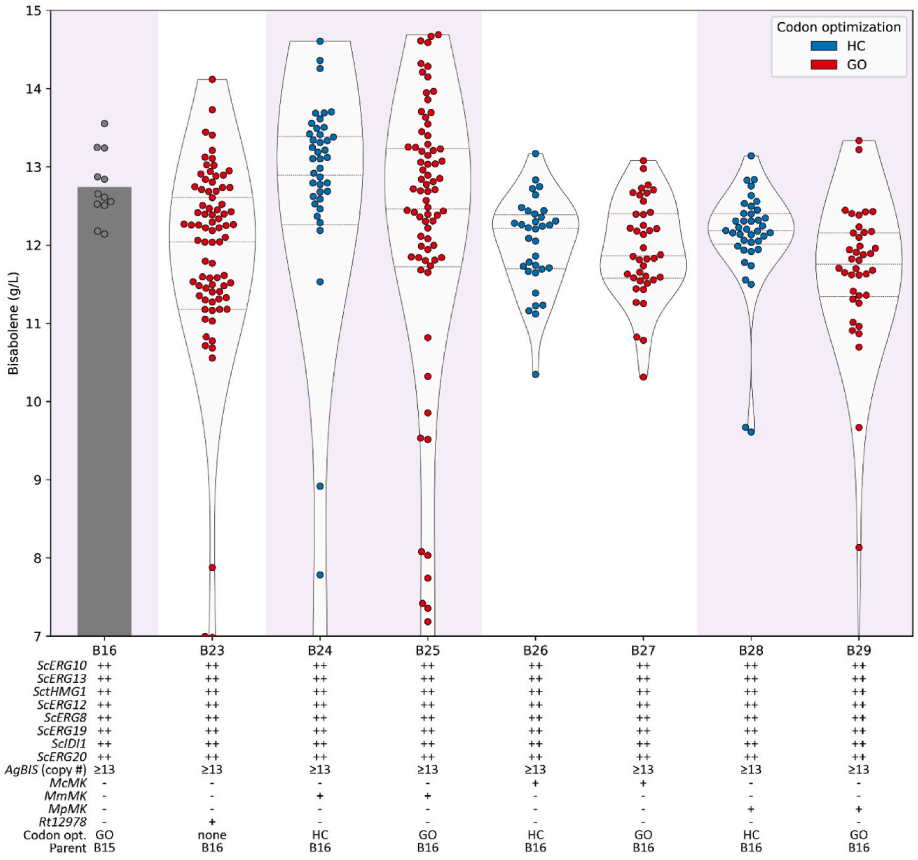

Fig. 9. Effect of feed-back inhibition resistant mevalonate kinases, codon optimization, and pentose catabolism upregulation on DMR final bisabolene titers in the parent strain B16 via random integration. The bar plot only displays biological replicates of a single strain (B16) (n = 13). All violin plots represent individual transformants (n = 89, 80, 48, 40, 34, 40, and 39 from left to right). MmMK, *Methanosarcina mazei* Go1 mevalonate kinase; McMK, *Methanosaeta concilii* GP-6 mevalonate kinase; MpMK, *Methanocella paludicola* SANAE mevalonate kinase.

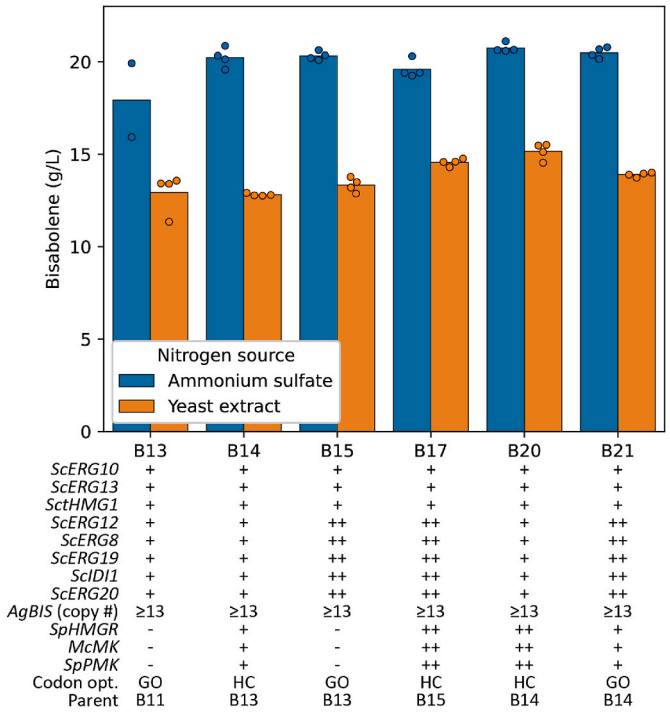

Fig. 10. Effect of alternative nitrogen sources on DMR bisabolene titers. Batch bisabolene titers on 300 g/L total sugar DMR supplemented with two nitrogen sources; n = 4 biological replicates. All individual points and bar plots represent biological replicates and their average, respectively.

3.8. Bioreactor cultivation

With success in microtiter batch scale, we decided to assess strain performance of the most highly engineered strain B22 in a fed-batch fermentation with a glucose synthetic defined medium at two scales (R1, 2 L and R2, 10 L) with identical pulsed glucose feeding strategies (Fig. 11). For nearly all metrics for all time points, R1 outperformed R2, likely due to mixing and mass transfer inefficiency, as noticed by overlay-aqueous phase separation in R2. Relative to the hydrolysate (R3), average R1 productivity (0.11 g/L/h), biomass reading (100 OD_{600}), and bisabolene titer (19.3 g/L) were 75%, 60%, and 5% higher, but with slightly lower yields (19% and 15% MTY for R1 and R2, respectively). Notably, the productivity for R1 is the highest reported in the literature for bisabolene in any system and host configuration. Interestingly, bisabolene production in R1 continued after depletion of sugars, presumably due to consumption of accumulated lipids.

Additionally, we completed two 2 L fed-batch bioreactor experiments with DMR (Supp Fig. 4). Certain C:N ratios strongly trigger lipogenesis and can possibly alter titers for AcCoA-derived bioproducts, so each experiment explored different pH adjustment and carbon feeding strategies; namely, ammonium hydroxide base with a separate pure glucose feed (R3) or sodium hydroxide base with a separate, mixed glucose and AS feed (R4). The peak aqueous-normalized titers 18.3 and 14.6 g/L for R3 and R4, respectively, were very similar considering a nearly 2-fold difference in peak biomass OD readings, corresponding to an estimated higher biomass yield of R3. However, it is unclear whether this corresponds to cell dry weight yields, as the effects of lipid accumulation (due to C:N ratios) and cell morphology on OD measurements is not well understood. See Supplementary Table 1 for a summary of bioreactor key metrics and process parameters.

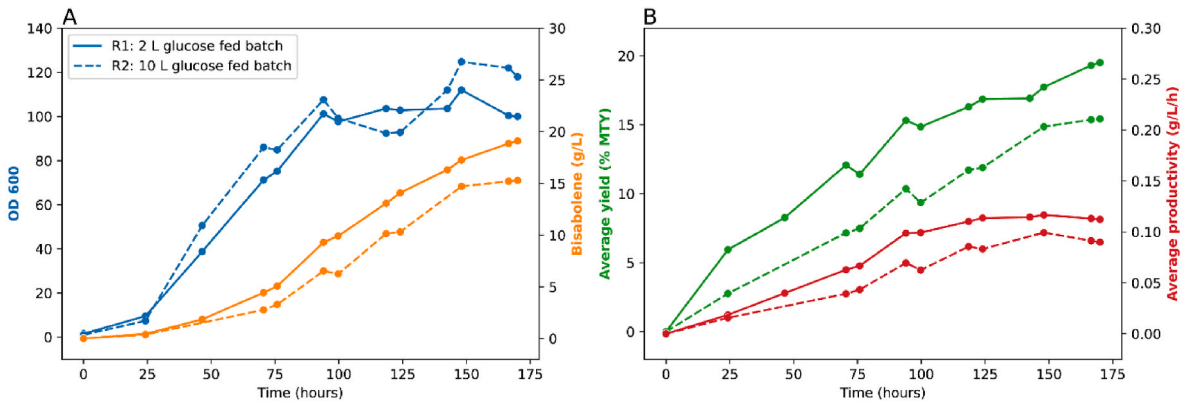

Fig. 11. Time-course key performances of glucose fed-batch bioreactor experiments of strain B22. Bioreactor runs with at 2 L and 10 L scales with an identical defined glucose medium feeding strategy starting with a minimal medium base recipe (R1 and R2, respectively). More details are included in Supplementary Table 1.

4. Discussion

Recently, a techno-economic analysis and life cycle assessment analysis combined with *R. toruloides* genome-scale metabolic modeling was completed for bisabolene production (Baral et al., 2024). Baseline cost modeling parameters were sorghum pretreated with ionic liquids followed by enzymatic saccharification to yield ~95 g/L glucose and ~68 g/L xylose, bisabolene at 90% MTY, and 36-h production time. This equates to ~40 g/L bisabolene, and a productivity of ~1.1 g/L/h, which far exceeds any published results. In a biorefinery without biogenic carbon dioxide and cell debris waste upgrading, the minimum selling price (MSP) of bisabolene (with no policy incentives) is over the projected 2050 conventional jet fuel price ($0.78/L) but under the high oil price scenario ($1.4/L). However, with policy incentives, cost parity MSP ($0.78/L) requires bisabolene yield ~30% MTY, ~13 g/L titer, and 0.37 g/L/h productivity. Sensitivity analysis on MSP concluded more effect from glucose bioconversion yields than xylose, that productivity adds ~$0.50/L for every 36 h of duration, and hydrogen cost (for alkene saturation) is the most influential factor determining MSP. Overall, this analysis allows us to benchmark our strains and indicates that with appropriate policy incentives, current titers, rates, and yields demonstrated in this work are nearly sufficient to reach cost parity.

With evident MVAP intermediate accumulation (Fig. 8), future work will systematically test feedback-resistant homologs of MK, PMK, and mevalonate diphosphate decarboxylase, as well as optimize MVAP expression levels. Peroxisomal MVAP compartmentalization to reduce competition with cytosolic MVA intermediates may prove useful (Gerke et al., 2020; Zhao et al., 2023). Additionally, non-intuitive targets remain to be explored including homologs of uncharacterized *S. cerevisiae* targets *ROX1*, a*yjl064w*, and *yjl062w* that improved yeast bisabolene titers (Giaever et al., 2002; Jakočiūnas et al., 2015; Özaydın et al., 2013). Moreover, in this study we have explored a range of trace metals and identified significant impacts from zinc. Further studies will be needed to understand how zinc regulates the pathways, as well as explore into MVAP transcriptional activator/repressor homologs and/or chemical regulation of competing squalene synthase (Bröker et al., 2018; Kaliszewski et al., 2008; Paddon et al., 2013). Furthermore, exploration of cost-effective genetic and non-genetic switches for biphasic growth-production (e.g., maltose switch utilized by Amyris) may further enable reduced costs in continuous fermentation (Moore et al., 2022; Pooth et al., 2020; Sandoval et al., 2014; Zhang et al., 2022). Similarly, to avoid possible redox imbalance and excess carbon loss via the oxidative pentose phosphate pathway, replacement of NADH-dependent HMG-CoA reductase and transhydrogenase expression is justified. Likewise, for every mol of bisabolene, 4 mol of carbon are lost via decarboxylation, prioritizing implementation of non-oxidative glycolysis to conserve carbon from glucose to AcCoA (Bogorad et al., 2013). These strategies are proven in *S. cerevisiae* to produce farnesene titers of ~105 g/L (Meadows et al., 2016).

Lignocellulosic feedstocks have increased sugar yield potential per land area and overall great abundance (Brown et al., 2024); however, second generation biofuels do not dominate over their first generation counterparts—bioethanol, biobutanol, biodiesel, and biogas—chiefly due to deconstruction and bioconversion difficulties. As such, we emphasize that biomass hydrolysate was the main carbon source in this work, highlighting the robustness of engineering *R. toruloides* for biofuels and biochemicals.

5. Conclusion

In this work, we explored combinatorial overexpression of the complete eight-gene *S. cerevisiae* MVAP, attenuation of competing fatty acid biosynthesis pathway, and process optimization in *R. toruloides* and achieved 20.8 g/L bisabolene in corn stover hydrolysate, the highest reported titer to the best of our knowledge. Multi-omic analysis determined that MK, PMK, and/or mevalonate diphosphate decarboxylase are the rate limiting enzymes due to accumulation of their upstream substrates and their qualitative protein abundance being the lowest amongst the MVAP. To reach cost parity with oil-derived fuels, future work will need to improve performance metrics via a multifaceted approach, including optimizing fermentation parameters, further rational engineering, mutagenesis, and strain sequencing. This work contributes to the generation of a terpene platform strain overexpressing MVA intermediates up to FPP, enabling versatile production of various terpenes including limonene, valencene, squalene, 2,3-oxidosqualene, and β-carotene.

CRediT authorship contribution statement

Paul A. Adamczyk: Writing – review & editing, Writing – original draft, Visualization, Validation, Methodology, Investigation, Formal analysis, Conceptualization. **Hee Jin Hwang:** Writing – review & editing, Writing – original draft, Visualization, Validation, Methodology, Investigation, Formal analysis, Conceptualization. **Ta-Hsuan Chang:** Validation, Investigation, Formal analysis. **Yuqian Gao:** Validation, Investigation, Formal analysis. **Edward E.K. Baidoo:** Validation, Investigation, Formal analysis. **Joonhoon Kim:** Validation, Formal analysis. **Bobbie-Jo M. Webb-Robertson:** Validation, Formal analysis. **Javier E. Flores:** Validation, Formal analysis. **Kirch Czarina Quijano:** Resources. **Meagan C. Burnet:** Resources. **Nathalie Munoz:** Resources. **Eric Sundstrom:** Supervision. **John M. Gladden:** Supervision, Project administration, Funding acquisition. **Di Liu:** Writing – review & editing, Supervision, Project administration, Funding acquisition.

Availability of data

The datasets generated during and/or analyzed during the current study are available from the corresponding author on reasonable request. All strains and plasmid sequences named in this work are available through the Agile BioFoundry parts registry at https://public-registry.agilebiofoundry.org.

Declarations of competing interest

None.

Acknowledgements

Sandia National Laboratories is a multi-mission laboratory managed and operated by National Technology and Engineering Solutions of Sandia LLC., a wholly-owned subsidiary of Honeywell International Inc., for the U.S. Department of Energy's National Nuclear Security Administration under contract DE-NA0003525. This study was part of the Agile BioFoundry (https://agilebiofoundry.org) supported by the U. S. Department of Energy, Energy Efficiency and Renewable Energy, Bioenergy Technologies Office, through contract DE-AC02-05CH11231 between Lawrence Berkeley National Laboratory and the U.S. Department of Energy. A portion of this research was performed on a project award (10.46936/reso.proj.2020.51637/60000235) from the Environmental Molecular Sciences Laboratory, a DOE Office of Science User Facility sponsored by the Biological and Environmental Research program under Contract No. DE-AC05-76RL01830. The views and opinions of the authors expressed herein do not necessarily state or reflect those of the United States Government or any agency thereof. Neither the United States Government nor any agency thereof, nor any of their employees, makes any warranty, expressed or implied, or assumes any legal liability or responsibility for the accuracy, completeness, or usefulness of any information, apparatus, product, or process disclosed or represents that its use would not infringe privately owned rights. The Department of Energy will provide public access to these results of federally sponsored research in accordance with the DOE Public Access Plan (http://energy.gov/downloads/doe-public-access-plan).

Appendix A. Supplementary data

Supplementary data to this article can be found online at https://doi.org/10.1016/j.ymben.2025.02.014.

Data availability

Data will be made available on request.

References

Adamczyk, P.A., Coradetti, S.T., Gladden, J.M., 2023. Non-canonical D-xylose and L-arabinose metabolism via D-arabitol in the oleaginous yeast Rhodosporidium toruloides. Microb. Cell Fact. 22, 145. https://doi.org/10.1186/s12934-023-02126-x.

Alexander, W.G., Doering, D.T., Hittinger, C.T., 2014. High-efficiency genome editing and allele replacement in prototrophic and wild strains of Saccharomyces. Genetics 198, 859–866. https://doi.org/10.1534/genetics.114.170118.

Amer, B., Kakumanu, R., Baidoo, E.E., 2022. HILIC-MS analysis of central carbon metabolites in gram negative bacteria v1. https://doi.org/10.17504/protocols.io.4r3l2opzxv1y/v1.

Andreassi, J.L., Dabovic, K., Leyh, T.S., 2004. Streptococcus pneumoniae isoprenoid biosynthesis is downregulated by diphosphomevalonate: an antimicrobial target. Biochemistry 43, 16461–16466. https://doi.org/10.1021/bi048075t.

Baral, N.R., Banerjee, D., Mukhopadhyay, A., Simmons, B.A., Singer, S.W., Scown, C.D., 2024. Integration of genome-scale metabolic model with biorefinery process model reveals market-competitive carbon-negative sustainable aviation fuel utilizing microbial cell mass lipids and biogenic CO2. Bioresources 19, 4056–4086. https://doi.org/10.15376/biores.19.3.4056-4086.

Baral, N.R., Kavvada, O., Mendez-Perez, D., Mukhopadhyay, A., Lee, T.S., Simmons, B.A., Scown, C.D., 2019. Techno-economic analysis and life-cycle greenhouse gas mitigation cost of five routes to bio-jet fuel blendstocks. Energy Environ. Sci. 12, 807–824. https://doi.org/10.1039/C8EE03266A.

Benjamini, Y., Hochberg, Y., 1995. Controlling the false discovery rate: a practical and powerful approach to multiple testing. J. Roy. Stat. Soc. B 57, 289–300. https://doi.org/10.1111/j.2517-6161.1995.tb02031.x.

Bogorad, I.W., Lin, T.-S., Liao, J.C., 2013. Synthetic non-oxidative glycolysis enables complete carbon conservation. Nature 502, 693–697. https://doi.org/10.1038/nature12575.

Bröker, J.N., Müller, B., van Deenen, N., Prüfer, D., Schulze Gronover, C., 2018. Upregulating the mevalonate pathway and repressing sterol synthesis in Saccharomyces cerevisiae enhances the production of triterpenes. Appl. Microbiol. Biotechnol. 102, 6923–6934. https://doi.org/10.1007/s00253-018-9154-7.

Brown, J., Lindstrom, J.K., Ghosh, A., Rollag, S.A., Brown, R.C., 2024. Production of sugars from lignocellulosic biomass via biochemical and thermochemical routes. Front. Energy Res. 12. https://doi.org/10.3389/fenrg.2024.1347373.

Burg, J.S., Espenshade, P.J., 2011. Regulation of HMG-CoA reductase in mammals and yeast. Prog. Lipid Res. 50, 403–410. https://doi.org/10.1016/j.plipres.2011.07.002.

Butcher, M.G., Meyer, P.A., Hallen, R.T., Albrecht, K.O., Clayton, C.K., Polikarpov, E., Rappe, K.G., Jones, S.B., Magnuson, J.K., 2018. Fungal metabolites as precursors to renewable transportation fuels. Fuel 215, 123–141. https://doi.org/10.1016/j.fuel.2017.10.052.

Carrigan, C.N., Poulter, C.D., 2003. Zinc is an essential cofactor for type I isopentenyl diphosphate:dimethylallyl diphosphate isomerase. J. Am. Chem. Soc. 125, 9008–9009. https://doi.org/10.1021/ja0350381.

Castañeda, M.T., Nuñez, S., Garelli, F., Voget, C., De Battista, H., 2018. Comprehensive analysis of a metabolic model for lipid production in Rhodosporidium toruloides. J. Biotechnol. 280, 11–18. https://doi.org/10.1016/j.jbiotec.2018.05.010.

Chen, X., Kuhn, E., Jennings, E.W., Nelson, R., Tao, L., Zhang, M., Tucker, M.P., 2016. DMR (deacetylation and mechanical refining) processing of corn stover achieves high monomeric sugar concentrations (230 g L−1)during enzymatic hydrolysis and high ethanol concentrations (>10% v/v)during fermentation without hydrolysate purification or concentration. Energy Environ. Sci. 9, 1237–1245. https://doi.org/10.1039/C5EE03718B.

Coradetti, S.T., Adamczyk, P.A., Liu, D., Gao, Y., Otoupal, P.B., Geiselman, G.M., Webb-Robertson, B.-J.M., Burnet, M.C., Kim, Y.-M., Burnum-Johnson, K.E., Magnuson, J., Gladden, J.M., 2023. Engineering transcriptional regulation of pentose metabolism in Rhodosporidium toruloides for improved conversion of xylose to bioproducts. Microb. Cell Fact. 22, 144. https://doi.org/10.1186/s12934-023-02148-5.

Coradetti, S.T., Pinel, D., Geiselman, G.M., Ito, M., Mondo, S.J., Reilly, M.C., Cheng, Y.-F., Bauer, S., Grigoriev, I.V., Gladden, J.M., Simmons, B.A., Brem, R.B., Arkin, A.P., Skerker, J.M., 2018. Functional genomics of lipid metabolism in the oleaginous yeast Rhodosporidium toruloides. Elife 7. https://doi.org/10.7554/eLife.32110.

Deshavath, N.N., Woodruff, W., Eller, F., Susanto, V., Yang, C., Rao, C.V., Singh, V., 2024. Scale-up of microbial lipid and bioethanol production from oilcane. Bioresour. Technol. 399, 130594. https://doi.org/10.1016/j.biortech.2024.130594.

Donald, K.A., Hampton, R.Y., Fritz, I.B., 1997. Effects of overproduction of the catalytic domain of 3-hydroxy-3-methylglutaryl coenzyme A reductase on squalene synthesis in Saccharomyces cerevisiae. Appl. Environ. Microbiol. 63, 3341–3344. https://doi.org/10.1128/aem.63.9.3341-3344.1997.

Dorsey, J.K., Porter, J.W., 1968. The inhibition of mevalonic kinase by geranyl and farnesyl pyrophosphates. J. Biol. Chem. 243, 4667–4670.

Ebrahim, A., Lerman, J.A., Palsson, B.O., Hyduke, D.R., 2013. COBRApy: COnstraints-based reconstruction and analysis for Python. BMC Syst. Biol. 7, 74. https://doi.org/10.1186/1752-0509-7-74.

Fernandes, M.A., Mota, M.N., Faria, N.T., Sá-Correia, I., 2023. An evolved strain of the oleaginous yeast Rhodotorula toruloides, multi-tolerant to the major inhibitors present in lignocellulosic hydrolysates, exhibits an altered cell envelope. J Fungi (Basel) 9. https://doi.org/10.3390/jof9111073.

Gao, L., Hou, R., Cai, P., Yao, L., Wu, X., Li, Y., Zhang, L., Zhou, Y.J., 2024. Engineering yeast peroxisomes for α-bisabolene production from sole methanol with the aid of proteomic analysis. JACS Au. https://doi.org/10.1021/jacsau.4c00106.

Gao, Y., Fillmore, T.L., Munoz, N., Bentley, G.J., Johnson, C.W., Kim, J., Meadows, J.A., Zucker, J.D., Burnet, M.C., Lipton, A.K., Bilbao, A., Orton, D.J., Kim, Y.-M., Moore, R.J., Robinson, E.W., Baker, S.E., Webb-Robertson, B.-J.M., Guss, A.M., Gladden, J.M., Beckham, G.T., Magnuson, J.K., Burnum-Johnson, K.E., 2020. High-throughput large-scale targeted proteomics assays for quantifying pathway proteins in Pseudomonas putida KT2440. Front. Bioeng. Biotechnol. 8, 603488. https://doi.org/10.3389/fbioe.2020.603488.

Geiselman, G.M., Kirby, J., Landera, A., Otoupal, P., Papa, G., Barcelos, C., Sundstrom, E. R., Das, L., Magurudeniya, H.D., Wehrs, M., Rodriguez, A., Simmons, B.A., Magnuson, J.K., Mukhopadhyay, A., Lee, T.S., George, A., Gladden, J.M., 2020a. Conversion of poplar biomass into high-energy density tricyclic sesquiterpene jet fuel blendstocks. Microb. Cell Fact. 19, 208. https://doi.org/10.1186/s12934-020-01456-4.

Geiselman, G.M., Zhuang, X., Kirby, J., Tran-Gyamfi, M.B., Prahl, J.-P., Sundstrom, E.R., Gao, Y., Munoz Munoz, N., Nicora, C.D., Clay, D.M., Papa, G., Burnum-Johnson, K. E., Magnuson, J.K., Tanjore, D., Skerker, J.M., Gladden, J.M., 2020b. Production of ent-kaurene from lignocellulosic hydrolysate in Rhodosporidium toruloides. Microb. Cell Fact. 19, 24. https://doi.org/10.1186/s12934-020-1293-8.

Gerke, J., Frauendorf, H., Schneider, D., Wintergoller, M., Hofmeister, T., Poehlein, A., Zebec, Z., Takano, E., Scrutton, N.S., Braus, G.H., 2020. Production of the fragrance geraniol in peroxisomes of a product-tolerant baker's yeast. Front. Bioeng. Biotechnol. 8, 582052. https://doi.org/10.3389/fbioe.2020.582052.

Giaever, G., Chu, A.M., Ni, L., Connelly, C., Riles, L., Véronneau, S., Dow, S., Lucau-Danila, A., Anderson, K., André, B., Arkin, A.P., Astromoff, A., El-Bakkoury, M., Bangham, R., Benito, R., Brachat, S., Campanaro, S., Curtiss, M., Davis, K.,

Deutschbauer, A., Entian, K.-D., Flaherty, P., Foury, F., Garfinkel, D.J., Gerstein, M., Gotte, D., Güldener, U., Hegemann, J.H., Hempel, S., Herman, Z., Jaramillo, D.F., Kelly, D.E., Kelly, S.L., Kötter, P., LaBonte, D., Lamb, D.C., Lan, N., Liang, H., Liao, H., Liu, L., Luo, C., Lussier, M., Mao, R., Menard, P., Ooi, S.L., Revuelta, J.L., Roberts, C.J., Rose, M., Ross-Macdonald, P., Scherens, B., Schimmack, G., Shafer, B., Shoemaker, D.D., Sookhai-Mahadeo, S., Storms, R.K., Strathern, J.N., Valle, G., Voet, M., Volckaert, G., Wang, C., Ward, T.R., Wilhelmy, J., Winzeler, E.A., Yang, Y., Yen, G., Youngman, E., Yu, K., Bussey, H., Boeke, J.D., Snyder, M., Philippsen, P., Davis, R.W., Johnston, M., 2002. Functional profiling of the Saccharomyces cerevisiae genome. Nature 418, 387–391. https://doi.org/10.1038/nature00935.

Gray, J.C., Kekwick, R.G., 1972. The inhibition of plant mevalonate kinase preparations by prenyl pyrophosphates. Biochim. Biophys. Acta 279, 290–296. https://doi.org/10.1016/0304-4165(72)90145-6.

Grigoriev, I.V., Nikitin, R., Haridas, S., Kuo, A., Ohm, R., Otillar, R., Riley, R., Salamov, A., Zhao, X., Korzeniewski, F., Smirnova, T., Nordberg, H., Dubchak, I., Shabalov, I., 2014. MycoCosm portal: gearing up for 1000 fungal genomes. Nucleic Acids Res. 42, D699–D704. https://doi.org/10.1093/nar/gkt1183.

Guerra, B., Recio, C., Aranda-Tavío, H., Guerra-Rodríguez, M., García-Castellano, J.M., Fernández-Pérez, L., 2021. The mevalonate pathway, a metabolic target in cancer therapy. Front. Oncol. 11, 626971. https://doi.org/10.3389/fonc.2021.626971.

Hewage, R.T., Tseng, C.-C., Liang, S.-Y., Lai, C.-Y., Lin, H.-C., 2023. Genome mining of cryptic bisabolenes that were biosynthesized by intramembrane terpene synthases from Antrodia cinnamomea. Philos. Trans. R. Soc. Lond. B Biol. Sci. 378, 20220033. https://doi.org/10.1098/rstb.2022.0033.

Jakočiūnas, T., Bonde, I., Herrgård, M., Harrison, S.J., Kristensen, M., Pedersen, L.E., Jensen, M.K., Keasling, J.D., 2015. Multiplex metabolic pathway engineering using CRISPR/Cas9 in Saccharomyces cerevisiae. Metab. Eng. 28, 213–222. https://doi.org/10.1016/j.ymben.2015.01.008.

Kaliszewski, P., Szkopińska, A., Ferreira, T., Swiezewska, E., Berges, T., Żołądek, T., 2008. Rsp5p ubiquitin ligase and the transcriptional activators Spt23p and Mga2p are involved in co-regulation of biosynthesis of end products of the mevalonate pathway and triacylglycerol in yeast Saccharomyces cerevisiae. Biochim. Biophys. Acta 1781, 627–634. https://doi.org/10.1016/j.bbalip.2008.07.011.

Kazieva, E., Yamamoto, Y., Tajima, Y., Yokoyama, K., Katashkina, J., Nishio, Y., 2017. Characterization of feedback-resistant mevalonate kinases from the methanogenic archaeons Methanosaeta concilii and Methanocella paludicola. Microbiology 163, 1283–1291. https://doi.org/10.1099/mic.0.000510.

Keita, V.M., Lee, Y.Q., Lakshmanan, M., Ow, D.S.-W., Staniland, P., Staniland, J., Savill, I., Tee, K.L., Wong, T.S., Lee, D.-Y., 2024. Evaluating oleaginous yeasts for enhanced microbial lipid production using sweetwater as a sustainable feedstock. Microb. Cell Fact. 23, 63. https://doi.org/10.1186/s12934-024-02336-x.

Kim, J., Coradetti, S.T., Kim, Y.-M., Gao, Y., Yaegashi, J., Zucker, J.D., Munoz, N., Zink, E.M., Burnum-Johnson, K.E., Baker, S.E., Simmons, B.A., Skerker, J.M., Gladden, J.M., Magnuson, J.K., 2020. Multi-omics driven metabolic network reconstruction and analysis of lignocellulosic carbon utilization in rhodosporidium toruloides. Front. Bioeng. Biotechnol. 8, 612832. https://doi.org/10.3389/fbioe.2020.612832.

Kirby, J., Geiselman, G.M., Yaegashi, J., Kim, J., Zhuang, X., Tran-Gyamfi, M.B., Prahl, J.-P., Sundstrom, E.R., Gao, Y., Munoz, N., Burnum-Johnson, K.E., Benites, V. T., Baidoo, E.E.K., Fuhrmann, A., Seibel, K., Webb-Robertson, B.-J.M., Zucker, J., Nicora, C.D., Tanjore, D., Magnuson, J.K., Skerker, J.M., Gladden, J.M., 2021. Further engineering of R. toruloides for the production of terpenes from lignocellulosic biomass. Biotechnol. Biofuels 14, 101. https://doi.org/10.1186/s13068-021-01950-w.

Koh, C.M.J., Liu, Y., Moehninsi, Du, M., Ji, L., 2014. Molecular characterization of KU70 and KU80 homologues and exploitation of a KU70-deficient mutant for improving gene deletion frequency in Rhodosporidium toruloides. BMC Microbiol. 14, 50. https://doi.org/10.1186/1471-2180-14-50.

Lin, Y.-H., Chien, W.-S., Duan, K.-J., 2010. Correlations between reduction–oxidation potential profiles and growth patterns of Saccharomyces cerevisiae during very-high-gravity fermentation. Process Biochem. 45, 765–770. https://doi.org/10.1016/j.procbio.2010.01.018.

Liu, C.-G., Qin, J.-C., Lin, Y.-H., 2017. Fermentation and redox potential. In: Jozala, A.F. (Ed.), Fermentation Processes. InTech. https://doi.org/10.5772/64640.

Liu, D., Hwang, H.J., Otoupal, P.B., Geiselman, G.M., Kim, Joonhoon, Pomraning, K.R., Kim, Y.-M., Munoz, N., Nicora, C.D., Gao, Y., Burnum-Johnson, K.E., Jacobson, O., Coradetti, S., Kim, Jinho, Deng, S., Dai, Z., Prahl, J.-P., Tanjore, D., Lee, T.S., Magnuson, J.K., Gladden, J.M., 2023. Engineering Rhodosporidium toruloides for production of 3-hydroxypropionic acid from lignocellulosic hydrolysate. Metab. Eng. 78, 72–83. https://doi.org/10.1016/j.ymben.2023.05.001.

Liu, S., Zhang, M., Ren, Y., Jin, G., Tao, Y., Lyu, L., Zhao, Z.K., Yang, X., 2021. Engineering Rhodosporidium toruloides for limonene production. Biotechnol. Biofuels 14, 243. https://doi.org/10.1186/s13068-021-02094-7.

Liu, Y., Yang, Q., Zhao, F., 2021. Synonymous but not silent: the codon usage code for gene expression and protein folding. Annu. Rev. Biochem. 90, 375–401. https://doi.org/10.1146/annurev-biochem-071320-112701.

Liu, Z., Radi, M., Mohamed, E.T.T., Feist, A.M., Dragone, G., Mussatto, S.I., 2021. Adaptive laboratory evolution of Rhodosporidium toruloides to inhibitors derived from lignocellulosic biomass and genetic variations behind evolution. Bioresour. Technol. 333, 125171. https://doi.org/10.1016/j.biortech.2021.125171.

Lopes, H.J.S., Bonturi, N., Kerkhoven, E.J., Miranda, E.A., Lahtvee, P.-J., 2020. C/N ratio and carbon source-dependent lipid production profiling in Rhodotorula toruloides. Appl. Microbiol. Biotechnol. 104, 2639–2649. https://doi.org/10.1007/s00253-020-10386-5.

Martin, V.J.J., Pitera, D.J., Withers, S.T., Newman, J.D., Keasling, J.D., 2003. Engineering a mevalonate pathway in Escherichia coli for production of terpenoids. Nat. Biotechnol. 21, 796–802. https://doi.org/10.1038/nbt833.

Meadows, A.L., Hawkins, K.M., Tsegaye, Y., Antipov, E., Kim, Y., Raetz, L., Dahl, R.H., Tai, A., Mahatdejkul-Meadows, T., Xu, L., Zhao, L., Dasika, M.S., Murarka, A., Lenihan, J., Eng, D., Leng, J.S., Liu, C.-L., Wenger, J.W., Jiang, H., Chao, L., Westfall, P., Lai, J., Ganesan, S., Jackson, P., Mans, R., Platt, D., Reeves, C.D., Saija, P.R., Wichmann, G., Holmes, V.F., Benjamin, K., Hill, P.W., Gardner, T.S., Tsong, A.E., 2016. Rewriting yeast central carbon metabolism for industrial isoprenoid production. Nature 537, 694–697. https://doi.org/10.1038/nature19769.

Moore, J.C., Ramos, I., Van Dien, S., 2022. Practical genetic control strategies for industrial bioprocesses. J. Ind. Microbiol. Biotechnol. 49. https://doi.org/10.1093/jimb/kuab088.

Nakayasu, E.S., Nicora, C.D., Sims, A.C., Burnum-Johnson, K.E., Kim, Y.-M., Kyle, J.E., Matzke, M.M., Shukla, A.K., Chu, R.K., Schepmoes, A.A., Jacobs, J.M., Baric, R.S., Webb-Robertson, B.-J., Smith, R.D., Metz, T.O., 2016. MPLEx: a robust and universal protocol for single-sample integrative proteomic, metabolomic, and lipidomic analyses. mSystems 1. https://doi.org/10.1128/mSystems.00043-16.

Nguyen, A.D., Pham, D.N., Chau, T.H.T., Lee, E.Y., 2021. Enhancing sesquiterpenoid production from methane via synergy of the methylerythritol phosphate pathway and a short-cut route to 1-Deoxy-D-xylulose 5-phosphate in methanotrophic bacteria. Microorganisms 9. https://doi.org/10.3390/microorganisms9061236.

Nicaud, J.-M., Coq, A.-M.C.-L., Rossignol, T., Morin, N., 2017. Protocols for monitoring growth and lipid accumulation in oleaginous yeasts. In: McGenity, T.J., Timmis, K. N., Nogales, B. (Eds.), Hydrocarbon and Lipid Microbiology Protocols, Springer Protocols Handbooks. Springer Berlin Heidelberg, Berlin, Heidelberg, pp. 153–169. https://doi.org/10.1007/8623_2014_40.

Nora, L.C., Wehrs, M., Kim, J., Cheng, J.-F., Tarver, A., Simmons, B.A., Magnuson, J., Harmon-Smith, M., Silva-Rocha, R., Gladden, J.M., Mukhopadhyay, A., Skerker, J. M., Kirby, J., 2019. A toolset of constitutive promoters for metabolic engineering of Rhodosporidium toruloides. Microb. Cell Fact. 18, 117. https://doi.org/10.1186/s12934-019-1167-0.

Ochoa-Viñals, N., Alonso-Estrada, D., Faife-Pérez, E., Chen, Z., Michelena-Alvarez, G., Martínez-Hernández, J.L., García-Cruz, A., Ilina, A., 2024. β-Carotene production from sugarcane molasses by a newly isolated Rhodotorula toruloides L/24-26-1. Arch. Microbiol. 206, 245. https://doi.org/10.1007/s00203-024-03973-x.

Otoupal, P.B., Ito, M., Arkin, A.P., Magnuson, J.K., Gladden, J.M., Skerker, J.M., 2019. Multiplexed CRISPR-cas9-based genome editing of rhodosporidium toruloides. mSphere 4. https://doi.org/10.1128/mSphere.00099-19.

Özaydın, B., Burd, H., Lee, T.S., Keasling, J.D., 2013. Carotenoid-based phenotypic screen of the yeast deletion collection reveals new genes with roles in isoprenoid production. Metab. Eng. 15, 174–183. https://doi.org/10.1016/j.ymben.2012.07.010.

Paddon, C.J., Westfall, P.J., Pitera, D.J., Benjamin, K., Fisher, K., McPhee, D., Leavell, M. D., Tai, A., Main, A., Eng, D., Polichuk, D.R., Teoh, K.H., Reed, D.W., Treynor, T., Lenihan, J., Fleck, M., Bajad, S., Dang, G., Dengrove, D., Diola, D., Dorin, G., Ellens, K.W., Fickes, S., Galazzo, J., Gaucher, S.P., Geistlinger, T., Henry, R., Hepp, M., Horning, T., Iqbal, T., Jiang, H., Kizer, L., Lieu, B., Melis, D., Moss, N., Regentin, R., Secrest, S., Tsuruta, H., Vazquez, R., Westblade, L.F., Xu, L., Yu, M., Zhang, Y., Zhao, L., Lievense, J., Covello, P.S., Keasling, J.D., Reiling, K.K., Renninger, N.S., Newman, J.D., 2013. High-level semi-synthetic production of the potent antimalarial artemisinin. Nature 496, 528–532. https://doi.org/10.1038/nature12051.

Park, J.O., Rubin, S.A., Xu, Y.-F., Amador-Noguez, D., Fan, J., Shlomi, T., Rabinowitz, J. D., 2016. Metabolite concentrations, fluxes and free energies imply efficient enzyme usage. Nat. Chem. Biol. 12, 482–489. https://doi.org/10.1038/nchembio.2077.

Peralta-Yahya, P.P., Ouellet, M., Chan, R., Mukhopadhyay, A., Keasling, J.D., Lee, T.S., 2011. Identification and microbial production of a terpene-based advanced biofuel. Nat. Commun. 2, 483. https://doi.org/10.1038/ncomms1494.

Peralta-Yahya, P.P., Zhang, F., del Cardayre, S.B., Keasling, J.D., 2012. Microbial engineering for the production of advanced biofuels. Nature 488, 320–328. https://doi.org/10.1038/nature11478.

Perez-Pimienta, J.A., Papa, G., Rodriguez, A., Barcelos, C., Liang, L., Stavila, V., Sanchez, A., Gladden, J., Simmons, B., 2019. Pilot-scale hydrothermal pretreatment and optimized saccharification enables bisabolene production from multiple feedstocks. Green Chem. https://doi.org/10.1039/C9GC00323A.

Pooth, V., van Gaalen, K., Trenkamp, S., Wiechert, W., Oldiges, M., 2020. Comprehensive analysis of metabolic sensitivity of 1,4-butanediol producing Escherichia coli toward substrate and oxygen availability. Biotechnol. Prog. 36, e2917. https://doi.org/10.1002/btpr.2917.

Primak, Y.A., Du, M., Miller, M.C., Wells, D.H., Nielsen, A.T., Weyler, W., Beck, Z.Q., 2011. Characterization of a feedback-resistant mevalonate kinase from the archaeon Methanosarcina mazei. Appl. Environ. Microbiol. 77, 7772–7778. https://doi.org/10.1128/AEM.05761-11.

Rodrigues, J.S., Lindberg, P., 2021. Metabolic engineering of Synechocystis sp. PCC 6803 for improved bisabolene production. Metab. Eng. Commun. 12, e00159. https://doi.org/10.1016/j.mec.2020.e00159.

Ro, D.-K., Paradise, E.M., Ouellet, M., Fisher, K.J., Newman, K.L., Ndungu, J.M., Ho, K. A., Eachus, R.A., Ham, T.S., Kirby, J., Chang, M.C.Y., Withers, S.T., Shiba, Y., Sarpong, R., Keasling, J.D., 2006. Production of the antimalarial drug precursor artemisinic acid in engineered yeast. Nature 440, 940–943. https://doi.org/10.1038/nature04640.

Sandoval, C.M., Ayson, M., Moss, N., Lieu, B., Jackson, P., Gaucher, S.P., Horning, T., Dahl, R.H., Denery, J.R., Abbott, D.A., Meadows, A.L., 2014. Use of pantothenate as a metabolic switch increases the genetic stability of farnesene producing

Saccharomyces cerevisiae. Metab. Eng. 25, 215–226. https://doi.org/10.1016/j.ymben.2014.07.006.
Shao, X., Zhou, J., Olson, D.G., Lynd, L.R., 2016. A markerless gene deletion and integration system for Thermoanaerobacter ethanolicus. Biotechnol. Biofuels 9, 100. https://doi.org/10.1186/s13068-016-0514-1.
Sivy, T.L., Fall, R., Rosenstiel, T.N., 2011. Evidence of isoprenoid precursor toxicity in Bacillus subtilis. Biosci. Biotechnol. Biochem. 75, 2376–2383. https://doi.org/10.1271/bbb.110572.
Spakowicz, D.J., Strobel, S.A., 2015. Biosynthesis of hydrocarbons and volatile organic compounds by fungi: bioengineering potential. Appl. Microbiol. Biotechnol. 99, 4943–4951. https://doi.org/10.1007/s00253-015-6641-y.
Sunder, S., Gupta, A., Kataria, R., Ruhal, R., 2024. Potential of rhodosporidium toruloides for fatty acids production using lignocellulose biomass. Appl. Biochem. Biotechnol. 196, 2881–2900. https://doi.org/10.1007/s12010-023-04681-w.
Trotta, E., 2013. Selection on codon bias in yeast: a transcriptional hypothesis. Nucleic Acids Res. 41, 9382–9395. https://doi.org/10.1093/nar/gkt740.
Tuller, T., Carmi, A., Vestsigian, K., Navon, S., Dorfan, Y., Zaborske, J., Pan, T., Dahan, O., Furman, I., Pilpel, Y., 2010. An evolutionarily conserved mechanism for controlling the efficiency of protein translation. Cell 141, 344–354. https://doi.org/10.1016/j.cell.2010.03.031.
Tuller, T., Zur, H., 2015. Multiple roles of the coding sequence 5' end in gene expression regulation. Nucleic Acids Res. 43, 13–28. https://doi.org/10.1093/nar/gku1313.
Vallee, B.L., Hoch, F.L., 1955. Zinc, a component of yeast alcohol dehydrogenase. Proc. Natl. Acad. Sci. U.S.A. 41, 327–338. https://doi.org/10.1073/pnas.41.6.327.
van der Horst, S., Filipovska, T., Hanson, J., Smeekens, S., 2020. Metabolite control of translation by conserved peptide uORFs: the ribosome as a metabolite multisensor. Plant Physiol. 182, 110–122. https://doi.org/10.1104/pp.19.00940.
Voynova, N.E., Rios, S.E., Miziorko, H.M., 2004. Staphylococcus aureus mevalonate kinase: isolation and characterization of an enzyme of the isoprenoid biosynthetic pathway. J. Bacteriol. 186, 61–67. https://doi.org/10.1128/JB.186.1.61-67.2004.
Walls, L.E., Otoupal, P., Ledesma-Amaro, R., Velasquez-Orta, S.B., Gladden, J.M., Rios-Solis, L., 2023. Bioconversion of cellulose into bisabolene using Ruminococcus flavefaciens and Rhodosporidium toruloides. Bioresour. Technol. 368, 128216. https://doi.org/10.1016/j.biortech.2022.128216.
Walls, L.E., Rios-Solis, L., 2020. Sustainable production of microbial isoprenoid derived advanced biojet fuels using different generation feedstocks: a review. Front. Bioeng. Biotechnol. 8, 599560. https://doi.org/10.3389/fbioe.2020.599560.
Webb-Robertson, B.-J.M., McCue, L.A., Waters, K.M., Matzke, M.M., Jacobs, J.M., Metz, T.O., Varnum, S.M., Pounds, J.G., 2010. Combined statistical analyses of peptide intensities and peptide occurrences improves identification of significant peptides from MS-based proteomics data. J. Proteome Res. 9, 5748–5756. https://doi.org/10.1021/pr1005247.
Wu, C.-C., Honda, K., Kazuhito, F., 2023. Current advances in alteration of fatty acid profile in Rhodotorula toruloides: a mini-review. World J. Microbiol. Biotechnol. 39, 234. https://doi.org/10.1007/s11274-023-03595-3.
Xie, Z.-T., Mi, B.-Q., Lu, Y.-J., Chen, M.-T., Ye, Z.-W., 2024. Research progress on carotenoid production by Rhodosporidium toruloides. Appl. Microbiol. Biotechnol. 108, 7. https://doi.org/10.1007/s00253-023-12943-0.
Yaegashi, J., Kirby, J., Ito, M., Sun, J., Dutta, T., Mirsiaghi, M., Sundstrom, E.R., Rodriguez, A., Baidoo, E., Tanjore, D., Pray, T., Sale, K., Singh, S., Keasling, J.D., Simmons, B.A., Singer, S.W., Magnuson, J.K., Arkin, A.P., Skerker, J.M., Gladden, J. M., 2017. Rhodosporidium toruloides: a new platform organism for conversion of lignocellulose into terpene biofuels and bioproducts. Biotechnol. Biofuels 10, 241. https://doi.org/10.1186/s13068-017-0927-5.
Yao, A., Choudhary, H., Mohan, M., Rodriguez, A., Magurudeniya, H., Pelton, J.G., George, A., Simmons, B.A., Gladden, J.M., 2021. Can multiple ions in an ionic liquid improve the biomass pretreatment efficacy? ACS Sustain. Chem. Eng. 12, 4371–4376. https://doi.org/10.1021/acssuschemeng.0c09330.
Yeo, S.K., Ali, A.Y., Hayward, O.A., Turnham, D., Jackson, T., Bowen, I.D., Clarkson, R., 2016. β-Bisabolene, a sesquiterpene from the essential oil extract of opoponax (Commiphora guidottii), exhibits cytotoxicity in breast cancer cell lines. Phytother Res. 30, 418–425. https://doi.org/10.1002/ptr.5543.
Zhang, G., Teng, M., Liu, S., Zhou, J., Li, J., Du, G., 2022. [Directed evolution of maltose induced promoters with expanded gradient intensity]. Sheng Wu Gong Cheng Xue Bao 38, 2606–2617. https://doi.org/10.13345/j.cjb.220251.
Zhang, Y., Song, X., Lai, Y., Mo, Q., Yuan, J., 2021. High-yielding terpene-based biofuel production in rhodobacter capsulatus. ACS Synth. Biol. 10, 1545–1552. https://doi.org/10.1021/acssynbio.1c00146.
Zhao, B., Zhang, Y., Wang, Y., Lu, Z., Miao, L., Wang, S., Li, Z., Sun, X., Han, Y., He, S., Zhang, Z., Xiao, D., Zhang, C., Foo, J.L., Wong, A., Yu, A., 2023. Biosynthesis of α-bisabolene from low-cost renewable feedstocks by peroxisome engineering and systems metabolic engineering of the yeast Yarrowia lipolytica. Green Chem. https://doi.org/10.1039/D3GC01936E.
Zhuang, X., Kilian, O., Monroe, E., Ito, M., Tran-Gymfi, M.B., Liu, F., Davis, R.W., Mirsiaghi, M., Sundstrom, E., Pray, T., Skerker, J.M., George, A., Gladden, J.M., 2019. Monoterpene production by the carotenogenic yeast Rhodosporidium toruloides. Microb. Cell Fact. 18, 54. https://doi.org/10.1186/s12934-019-1099-8.